AIAA 2002-1516

BUCKLING BEHAVIOR OF COMPRESSION-LOADED COMPOSITE CYLINDERICAL SHELLS WITH REINFORCED CUTOUTS

Mark W. Hilburger* and James H. Starnes, Jr.†
NASA Langley Research Center
Hampton, Virginia 23681-001

Abstract

Results from a numerical study of the response of thin-wall compression-loaded quasi-isotropic laminated composite cylindrical shells with reinforced and unreinforced square cutouts are presented. The effects of cutout reinforcement orthotropy, size, and thickness on the nonlinear response of the shells are described. A high-fidelity nonlinear analysis procedure has been used to predict the nonlinear response of the shells. The analysis procedure includes a nonlinear static analysis that predicts stable response characteristics of the shells and a nonlinear transient analysis that predicts unstable dynamic buckling response characteristics. The results illustrate how a compression-loaded shell with an unreinforced cutout can exhibit a complex nonlinear response. In particular, a local buckling response occurs in the shell near the cutout and is caused by a complex nonlinear coupling between local shell-wall deformations and in-plane destabilizing compression stresses near the cutout. In general, the addition of reinforcement around a cutout in a compression-loaded shell can retard or eliminate the local buckling response near the cutout and increase the buckling load of the shell, as expected. However, results are presented that show how certain reinforcement configurations can actually cause an unexpected increase in the magnitude of local deformations and stresses in the shell and cause a reduction in the buckling load. Specific cases are presented that suggest that the orthotropy, thickness, and size of a cutout reinforcement in a shell can be tailored to achieve improved response characteristics.

Introduction

Thin-walled cylindrical shells with cutouts are found in many aerospace structural applications. Advanced material systems are being used to produce stronger, lighter-weight aerospace shell structures, and improved analysis and design methods appropriate for these advanced material systems are needed. The high strength-to-weight and high stiffness-to-weight ratios of advanced composite materials offer significant weight reduction potential for aerospace structures. In addition, the use of advanced composite materials allows the designer to tailor the stiffness properties of the structure to obtain a structurally efficient design. Many aerospace shell structures have cutouts or openings that serve as doors, windows, or access ports and these cutouts or openings often require some type of reinforcing structure to control local structural deformations and stresses near the cutout. In addition, these structures may experience compression loads during operation, and thus their buckling response characteristics must also be understood and accurately predicted in order to determine safe operating conditions and effective designs for these structures.

Many studies have been conducted which show that a cutout in an isotropic shell structure can have a significant effect on the response of the shell. In particular, results indicate that a cutout in a shell structure causes a local response to occur near the cutout when the shell is subjected to load. This local response can consist of large out-of-plane deformations, large-magnitude rapidly varying stresses near the cutout (e.g., Refs. 1-2). If the load is a compressive load, the cutout can cause a local buckling response to occur in the shell at applied loads lower than the general instability load of the corresponding shell without a cutout (e.g., Refs. 3-5). For some cases, this local buckling response results in a stable postbuckling response localized near the cutout and additional load can be applied to the shell before it exhibits global collapse. For other cases, the local response in the shell causes a disturbance in the shell of sufficient magnitude to cause global collapse to occur immediately after the local instability occurs.

Significantly fewer studies have been conducted on the response of compression-loaded composite cylindrical shells with cutouts. Recent numerical and experimental studies of the response of compression-loaded composite cylindrical shells with unreinforced rectangular cutouts have been presented by Hilburger, et al.[6,7] In particular, their results have shown that localized regions of biaxial in-plane compression stresses form in the shell near the cutout, and these regions of biaxial stresses couple with the out-of-plane deforma-

*Aerospace Engineer, Mechanics and Durability Branch. Member, AIAA.
†Senior Engineer, Structures and Materials Competency. Fellow, AIAA.

tions of the shell wall causing an unstable local buckling response to occur near the cutout. In addition, their results indicate that laminate orthotropy can have a significant effect on the nonlinear response and the buckling behavior of a shell with a cutout, as expected. For example, numerical results from Ref. 6 indicate that the normalized buckling load* of a $[\pm 45/0/90]_s$ quasi-isotropic shell with a 1.0-in. by 1.0-in. square cutout is approximately 33% lower than the normalized buckling load of a corresponding $[\pm 45/0_2]_s$ orthotropic shell with the same sized cutout. The large reduction in the normalized buckling load of the quasi-isotropic shell, as compared to the orthotropic shell, is caused by larger magnitude radial deformations and destabilizing in-plane compression stresses that develop near the cutout in the shell at a lower applied load level. These localized deformations and in-plane stresses cause the local buckling of the shell to initiate at a lower applied load level. These numerical results were verified with several experiments and the results indicated good agreement.

Similarly, very little information is available on the response of compression-loaded curved shells with reinforced cutouts, and the few results that do exist are limited to isotropic shells (e.g., Refs. 8-10). For example, Almroth and Holmes[8] presented results from a numerical and experimental study on the response of compression-loaded cylindrical shells with reinforced and unreinforced rectangular cutouts. Their results showed that the arrangement of the cutout reinforcement, that is, whether the reinforcement is positioned along an axially aligned free-edge or around all the edges of the cutout, can have a significant effect on the buckling response of the shell. Experimental results from Toda[10] indicate that, for certain sized circular cutouts in a compression-loaded cylindrical shell, the bucking load increased with an increase in the size of the reinforcement around the cutout. However, further reinforcement of the cutout beyond a certain amount did not always produce higher buckling loads, and in some cases further reinforcement caused a decrease in the buckling load of the shell.

A simplified design-level analysis procedure and empirical data are often used in the design of shells with reinforcements. The traditional method for the preliminary design of a reinforced cutout in a thin-walled shell structure is based on the linear analysis of a flat plate with a square cutout (e.g., Ref. 11) and the effects of shell curvature and other modeling approximations are taken into account by applying empirical correction factors. However, this design method may not be sufficient for the design of large cutouts in curved shell structures because of the lack of accuracy in the analysis and the complex nonlinear behavior exhibited by these types of structures. In addition, this design method can result in overly conservative designs or unconservative designs for these structures if the empirical correction factors are not applicable to the design of interest. For example, current design practice does not include information or design procedures for the design of reinforced cutouts in composite shell structures.

A review of the results presented in the literature indicates that the response of a compression-loaded cylindrical shell with an unreinforced cutout is, for the most part, understood. In contrast, the effects of cutout reinforcement on the buckling behavior of compression-loaded composite cylindrical shells, is not well understood. The objective of this paper is to identify the typical nonlinear response characteristics of a compression-loaded, thin-walled, quasi-isotropic, laminated, cylindrical shell with a square cutout and to illustrate the effects of several cutout reinforcement configurations on the response. This thin-walled cylindrical shell configuration was chosen as a generic example of a typical aerospace shell structure with a cutout subjected to a destabilizing load. Numerical results that show the effects of 18 different reinforcement configurations on the response of these shell structures are presented. The various cutout reinforcement configurations considered were used to study the effects of reinforcement orthotropy, thickness, and size on the response of the shell. In addition, the results are used to illustrate the feasibility of structurally tailoring cutout reinforcement to control shell-wall deformations and stresse concentrations near a cutout in a compression-loaded shell and to increase the load carrying capacity of the shell. A modern high-fidelity nonlinear analysis procedure is used in the study (e.g., Ref. 12) that offers the opportunity to provide insight into the effects of various cutout reinforcement concepts on the response of compression-loaded shell structures. This procedure also offers the opportunity to improve some of the engineering approximations and methods that are used in the design of reinforced cutouts in shell structures. The high-fidelity nonlinear analysis procedure used in this study has been successfully applied to the analysis of other similar compression-loaded shells with cutouts and the predicted results have been verified with selected experiments, e.g., see Ref. 7. First, results illustrating the response of a compression-loaded cylinder with an unreiforced cutout are presented. Then, results illustrating the effects

* The normalized buckling load is defined as the buckling load of the shell with a cutout predicted from a nonlinear analysis normalized with respect to the buckling load of the corresponding shell without a cutout predicted from a linear bifurcation analysis.

of selected cutout reinforcement on the response of the shell are presented. Lastly, response trends are identified and discussed. The results include load-shortening response curves; prebuckling, buckling and postbuckling deformation patterns; and prebuckling, buckling, and postbuckling stress contours.

Finite-Element Models and Analyses

Nonlinear Analysis Procedure

The shells considered in this study were analyzed with the STAGS (STructural Analysis of General Shells) nonlinear shell analysis code.[13] STAGS is a finite-element code designed for the static and dynamic analysis of general shells, and includes the effects of geometric and material nonlinearities in the analysis. The STAGS code uses both the modified and full Newton methods for its nonlinear solution algorithms, and accounts for large rotations in a shell wall by using a corotational algorithm implemented at the element level. The Riks pseudo arc-length path-following method[14] is used to continue a solution past the limit points of a nonlinear response. With this strategy, the incrementally applied loading parameter is replaced by an arc-length along the solution path, which is then used as the independent loading parameter. The arc-length increments are automatically adjusted by the program as a function of the solution behavior. A transient analysis option is included in STAGS that uses an implicit numerical time-integration method developed by Park[15] and proportional structural damping. Mass and stiffness damping factors used in the transient analysis are defined as $\alpha=2\pi\nu\zeta$, and $\beta=\zeta/2\pi\nu$, respectively, where ζ denotes the fraction of critical damping and is assumed to equal 0.15 for these shells. The dynamic buckling response of the shell is assumed to be dominated by a particular frequency of vibration, ν, and is defined as the critical frequency of vibration determined from a linear vibration analysis in STAGS. Additional information on the transient analysis in STAGS can be found in Ref. 16.

The prebuckling, buckling and postbuckling responses of the shells were determined by using the following analysis procedure. The quasi-static responses were determined by using the geometrically nonlinear quasi-static analysis capability in STAGS. The Riks pseudo arc-length path-following method was used to compute the response of the shell up to the buckling point. The unstable buckling response of the shell was predicted by using the nonlinear transient analysis option of the code. The transient analysis was initiated from an unstable equilibrium state close to the buckling point by incrementing the end displacement by a small amount, approximately 1%. An initial time step of 10^{-8} seconds was used in the analysis and is automatically adjusted by the program as a function of the solution behavior. The transient analysis was continued until the kinetic energy in the shell dissipated to a negligible level, which indicates that the transient response has attenuated. Once the transient analysis had attenuated to a near-steady-state solution, the load relaxation option of the code was used to establish a stable static equilibrium state. Conventional linear bifurcation buckling analysis results were also determined with STAGS for comparison with the nonlinear response results.

Finite-Element Models

Nineteen shells were analyzed in the present study and include one shell with an unreinforced cutout and 18 shells with reinforced cutouts; these shells are referred to herein as shells C1 through C19. A list of shell identification codes and corresponding reinforcement configurations is given in Table 1. The shells considered in the present study are modeled as geometrically perfect 8-ply laminated quasi-isotropic circular cylinders with a square cutout and subjected to a uniform axial end-shortening. The shells have a length of 16.0 in., a radius of 8.0 in., and shell-wall thickness of 0.04 in. that give a shell-radius-to-thickness ratio of 200. The cutout is a 1.0 in. by 1.0 in. square-shaped cutout with 0.05-in-radius reentrant corners. The shell wall was modeled as a $[\pm 45/0/90]_s$ quasi-isotropic laminate, in which each lamina ply had a thickness of 0.005 in. and a fiber volume fraction of 0.62. The material properties of a lamina ply are as follows: longitudinal compression modulus $E_1 = 18.5$ Msi, transverse modulus $E_2 = 1.64$ Msi, in-plane shear modulus $G_{12} = 0.87$ Msi, and major Poisson's ratio $\nu_{12} = 0.30$. Shells C2 through C19 include various forms of reinforcement around the cutout. The cutout reinforcement consists of additional square-shaped lamina plies added to the shell-wall laminate at the shell-wall mid-surface and are aligned concentrically with respect to the square-shaped cutout in the shell. Eighteen different reinforcement configurations were considered in which the reinforcement thickness, size, and ply-orientation were varied. Specifically, three different reinforcement thickness of 0.005 in., 0.01 in., and 0.02 in., corresponding to one, two, and four-ply reinforcement thicknesses, respectively, were considered. Two reinforcement ply orientations of 0° and 90° (a 0° ply and a 90° ply correspond to lamina plies with fibers aligned along the length of the shell and around its circumference, respectively) were considered. Three reinforcement sizes: a 2.4-in. by 2.4-in. square reinforcement, a 4.4-in. by 4.4-in. square reinforcement, and a 8.0-in. by 8.0-in. square reinforcement.

A typical finite-element model of a specimen is

shown in Fig. 1. The standard 410 quadrilateral element from the STAGS element library was used in the models. Typically, the elements of the finite-element mesh are approximately 0.2-in. by 0.2-in. square, but the mesh is refined near the cutout. Each element possesses four integration points, which are distributed to provide a modeling resolution of at least 0.1-in. Results from a mesh convergence study indicated that this degree of mesh refinement mesh was required to accurately model the bending boundary layer deformation response near the ends of the shell, the prebuckling short wavelength deformation response and rapidly varying stress distributions exhibited by the shells near the cutout, and the short wavelength deformation response and rapidly varying stress distributions exhibited by the shells during the transient buckling process. Clamped end conditions were used in the finite-element models in which the circumferential and radial displacements v and w are set equal to zero in end regions of the shell as indicated in Fig. 1. A typical finite-element model contained approximately 120,000 degrees of freedom.

Results and Discussion

Numerically predicted results for selected compression-loaded quasi-isotropic laminated cylindrical shells with reinforced and unreinforced cutouts are presented in this section. The results were obtained from finite-element models of geometrically perfect shells subjected to a uniform axial end-shortening. These results are presented to illustrate the overall behavior of a compression-loaded graphite-epoxy shell with a cutout and the effects of cutout reinforcement on the response. First, results illustrating the nonlinear response of a compression-loaded geometrically perfect quasi-isotropic cylindrical shell with an unreinforced square-shaped cutout are presented. Then, results illustrating the predicted response of selected compression-loaded cylindrical shells with reinforced cutouts are presented and compared. The results include load-shortening response curves; prebuckling, buckling and postbuckling deformation patterns; and prebuckling, buckling, and postbuckling stress contours.

Cylindrical Shell with an Unreinforced Cutout

Results for a quasi-isotropic shell with a 1.0-in by 1.0-in unreinforced square-shaped cutout, referred to herein as shell C1, are presented in this section to illustrate typical response characteristics of a compression-loaded shell with a square cutout. The numerically predicted load-shortening response curve for shell C1 is shown in Fig. 2a. The quasi-static response is indicated by a solid line and the unstable, transient buckling responses are indicated by the dashed lines in the figure. The axial load P is normalized with respect to the bifurcation buckling load predicted from a linear eigenvalue analysis of the corresponding shell without a cutout, P_{cr} = 42,590 lbf, and the end-shortening displacement Δ is normalized with respect to the shell length, L. The shell exhibits a complex nonlinear response as indicated by the numerous stable and unstable segments of the load-shortening response curve. The shell has a linear prebuckling response and a distinct buckling point labeled A at a normalized load level of $P/P_{cr} = 0.51$. The buckling response is characterized by a local, unstable transient buckling response in the shell and includes the formation of large magnitude radial deformations and rapidly varying stresses in the shell wall near the cutout. The shell exhibits a relatively small reduction in axial load, approximately 6%, during buckling and is indicated by the dashed line-segment A-B of the load-shortening response curve. The figure also presents a second solution path from point A to point B. This path corresponds to the quasi-static solution predicted by the arc-length path-following method. The results indicate that the quasi-static analysis and the transient analysis predict the same local postbuckling state at point B. During the prebuckling response, regions of destabilizing in-plane biaxial compression stresses form near the cutout and couple with the radial deformations near the cutout to cause the unstable local buckling response in the shell. A stable postbuckling response is exhibited by the shell as indicated by segment B-C of the load-shortening response. As loading continues in the postbuckling region of the response, the magnitude of the shell-wall radial deformations near the cutout increases. In addition, the results indicate that the slope of the postbuckling curve decreases as loading continues in the postbuckling range, indicating a reduction in effective axial stiffness. This decrease in effective axial stiffness is caused by increasingly large radial deformations that develop in the shell that causes a significant redistribution of load away from the cutout to reduce the effective, load-carrying cross-section of the shell. The global collapse of the shell occurs at point C and the unstable collapse response is represented in Fig. 2b by the dashed line segment C-F. The collapse response is characterized by a significant reduction in load and the development of the general instability mode. The transient nature of the unstable buckling responses in the shell is indicated by the load-time history of the collapse response of the shell shown in Fig. 2b. The load history curve exhibits a sudden reduction in axial load supported by the shell from $P/P_{cr} = 0.51$, at time t = 0.0 seconds, to $P/P_{cr} = 0.32$, at time t = 0.006 seconds into the transient response. In addition, the kinetic energy in the shell increases rapidly during the initial collapse re-

sponse and then dissipates as time progresses until the shell reaches a stable postbuckling equilibrium configuration. The shell obtains a stable postbuckling configuration after approximately 0.015 second have elapsed and the normalized postbuckling load value for the shell is equal to 0.33.

Deformation patterns corresponding to selected points during the compression response are shown in Figs. 3a-3f, and deformation patterns with superimposed axial and circumferential stress contours corresponding to selected points during the compression response are shown in Figs. 4a-4c (the magnitude of the deformation responses in these figures are exaggerated for clarity). The deformation response incipient to local buckling, (associated with point A in Fig. 2a), shown in Fig. 3a, is characterized by two ellipse-shaped inward buckles near the cutout with the semi-major axis of the buckles aligned in a helical or skew direction. The magnitude of the shell-wall radial deformations vary between -0.65 and +0.40 times the shell-wall thickness, where positive- and negative-valued displacements correspond to outward and inward radial displacements, respectively. The skewing of the deformation pattern is attributed to the presence of laminate anisotropy in the form of coupling between the bending and twisting of the shell wall. The axial and circumferential membrane stress contours indicate significant stress concentrations near the cutout that rapidly decay to far-field values away from the cutout, as shown in Fig. 4a (magnified views of the stresses near the cutout are shown for clarity). The maximum value of the axial compression stress resultant occurs at the corners of the cutout (-2023 lb/in.) and is equal to 4.7 times the corresponding uniform far-field value. Similarly, large magnitude circumferential stress concentrations occur near the cutout with stress resultant values that range between -695 lb/in. and +528 lb/in; the maximum circumferential tension stress resultant occurs at the mid-point of the upper and lower free-edges of the cutout and the maximum circumferential compression stress resultant occurs at the cutout corners. In addition, regions of localized circumferential compression stress resultant develop approximately 0.5 inches above and below the cutout with maximum stress resultant levels of approximately -110 lb/in. The local buckling response of the shell is initiated by a nonlinear coupling between localized destabilizing compressive axial and circumferential stress resultants and the radial deformations that occur in the shell near the cutout (e.g., Fig. 4a). The locations where local buckling initiates are marked by **X** symbols in Fig. 4a. The initial postbuckling deformation pattern associated with point B in Fig. 2a is shown in Fig. 3b and is characterized by large ellipse-shaped buckles on either side of the cutout. The magnitude of the shell-wall radial deformations have increased significantly and vary between -4.5 and +1.5 times the shell-wall thickness. As loading continues in the postbuckling range, the ellipse-shaped buckles in the shell wall increase in size and the buckle pattern rotates clockwise around the cutout, as shown in Fig. 3c. The magnitude of the shell-wall radial deformations increases to between -8.65 and +4.2 times the shell-wall thickness and a significant redistribution of the load in the shell occurs near the buckles, as shown in Fig. 4b. More specifically, the axial stress resultant distribution indicates a significant unloading of the shell near the inward buckles. This load redistribution coincides with the reduction in postbuckling stiffness indicated in Fig. 2a and causes a reduction in the effective, load-carrying cross-section of the shell. Moreover, a significant increase in the magnitude of the circumferential compression stress resultants occurs in the buckles. At the onset of global collapse, the shell-wall deformations change in a very short period of time from the stable, local deformation pattern shown in Fig. 3c to a unstable transient deformation pattern shown in Fig. 3d. Moreover, additional buckles form in the shell wall around the circumference of the shell. As the buckling process continues, there is a significant reduction in the axial load supported by the shell, and even more buckles develop in the shell wall, as indicated in Fig. 3e. After approximately 0.015 seconds have elapsed, the kinetic energy in the shell has dissipated to a negligible level, and the shell has deformed into a stable post-collapse general instability mode-shape that consists of eight buckles distributed around the circumference of the shell as shown in Fig. 3f. The corresponding post-collapse axial and circumferential stress resultant distribution patterns are shown in Fig. 4c and indicate significant stress resultant redistribution throughout the entire cylinder. In particular, the results indicate that the majority of the applied axial compression load is now supported by the ridges between the adjacent inward buckles in the shell wall, and alternating bands of circumferential tension and compression stress resultants are present in the shell.

Effects of Cutout Reinforcement

Results for eighteen compression-loaded quasi-isotropic shells with 1.0-in by 1.0-in square reinforced cutouts are presented in this section to identify the effects of selected cutout reinforcement configurations on the response of the shells (identified herein as shells C2-C19). The results for these shells are compared to results for the corresponding shell with an unreinforced cutout, shell C1, presented in the previous section.

The buckling results for the compression-loaded shell with an unreinforced cutout, shell C1, presented in

the previous section, identified several features of the behavior that are associated with the local buckling response of the shell. Most significantly, the nonlinear interaction between localized radial deformations and destabilizing biaxial stresses near the cutout cause the local buckling response of the shell to occur. This fundamental behavioral feature suggests that it may be possible to identify a cutout reinforcement configuration that retards the onset of the local deformations and destabilizing stress in the shell near the cutout and can retard or eliminate the onset of the local buckling response in the shell. To this end, a numerical parametric study was conducted to identify the effects of selected cutout reinforcement configurations on the response of a compression-loaded shell with a cutout. In particular, cutout reinforcement size, thickness, and orthotropy were studied. All of the reinforcements considered herein consist of square-shaped concentrically aligned lamina plies added to the shell-wall laminate at the shell-wall mid-surface. Thus, three reinforcement sizes were investigated to identify the effects of reinforcement size in the deformation response and stress distribution in the shell. The three square-shaped reinforcement sizes include 2.4-in. by 2.4-in, 4.4-in. by 4.4-in, and 8.0-in by 8.0-in square reinforcement (referred to herein as 2.4-in-square reinforcement, 4.4-in-square reinforcement, and 8.0-in-square reinforcement, respectively). Three reinforcement thicknesses were studied and include reinforcement thickness equal to 0.005 in., 0.01 in., and 0.02 in., corresponding to one-, two-, and four-ply reinforcements, respectively. Two reinforcement ply orientations of 0^o and 90^o (a 0^o-ply and a 90^o-ply correspond to lamina plies with fibers aligned along the length of the shell and around its circumference, respectively) were investigated to study the effects of reinforcement orthotropy on the response. A list of shell identification codes and corresponding reinforcement configurations is given in Table 1.

2.4-in. Square Reinforcement. Results from shells C2 through C7 are presented in this section. The cutout reinforcements for shells C2 through C4 and shells C5 through C7 consist of 0^o and 90^o 2.4-in. square-shaped lamina plies, respectively. Shells C2 and C5 have 0.005-in-thick reinforcement, shells C3 and C6 have 0.01-in-thick reinforcement, and shells C4 and C7 have 0.02-in-thick reinforcement. Numerically predicted load-shortening response curves for shells C2 through C4 and shells C5 through C7, are presented in Figs. 5a and 5b, respectively, and the results for the corresponding unreinforced shell, C1, are shown for comparison. The quasi-static responses are indicated by the solid lines and the unstable, transient buckling responses are indicated by the dashed lines in the figures. The axial load P is normalized with respect to the bifurcation buckling load of the corresponding shell without a cutout predicted from a linear eigenvalue analysis P_{cr} = 42,590 lbf, and the end-shortening displacement Δ is normalized with respect to the shell length L. The local buckling points are marked with filled circles, and global collapse points are indicated by an **X**. Curves showing the unstable transient responses associated with local buckling (e.g., line segment A-B shown in Fig. 2a for shell C1) for shells C1, C2, and C5 are omitted from Figs. 5a and 5b for clarity. The results show that the addition of reinforcement around the cutout can have a significant effect on the overall character of the load-shortening response of the shell. In particular, the results indicate that the local buckling loads can increase significantly as the thickness of the reinforcement is increased. More specifically, the normalized buckling loads for shells C2, C3, and C4 are equal to 0.57, 0.64, and 0.78, respectively, as compared to the buckling load of 0.51 for the corresponding unreinforced shell C1. Similarly, the normalized buckling loads for shells C5, C6, and C7 are equal to 0.59, 0.67, and 0.77, respectively. However, the results indicate that some of the shells with thicker reinforcement, shells C3, C4, C6, and C7, no longer exhibit stable post-local-buckling responses. For these shells, the local buckling response in these shell causes enough of a disturbance in the shell to cause the global collapse of the shell. In contrast, shells C2, and C4 exhibit stable post-local-buckling response and can support additional load before global collapse occurs. Upon global collapse, each shell obtains a stable post-collapse configuration and exhibits a significant reduction in axial load-carrying capability. The normalized post-collapse load levels for shell C2-C7 range from 0.32 to 0.35. For the most part, the results presented in Figs. 5a and 5b indicate that the cutout reinforcement orientation, that is 0^o-ply orientation versus 90^o-ply orientation, has a small effect (at most a 5% difference) on the buckling load of the shell and a negligable effect on the effective axial stiffness of the shell for this size reinforcement.

Displacement contour patterns just before buckling for shells C2-C4 are shown in Figs. 6a-6c, respectively. The radial displacements w are normalized with respect to the shell-wall thickness t = 0.04 in. The outer boundaries of the cutout reinforcement in each shell is marked in the figures with solid lines. The results indicate that the character of the deformation response in the shell incipient to buckling changes significantly as the thickness of the cutout reinforcement increases. In particular, the displacement contour patterns exhibited by shells C2 and C3 in Figs. 6a and 6b, respectively, in-

dicate similar local deformation response as that exhibited by shell C1 which is characterized by two ellipse-shaped inward buckles near the cutout. The semi-major axis of the buckles are aligned in a helical direction and the localized displacement gradients rapidly attenuate away from the cutout. However, the magnitudes of the shell-wall deformations decrease as the thickness of the reinforcement increases; that is, the magnitude of the normalized displacements range between -0.51 to 0.3 and -0.33 to 0.29 for shells C2 and C3, respectively, as compared to -0.65 to 0.4 for shell C1. These results correspond to as much as 21% and 49% reductions in the magnitude of the local deformations near the cutout for shells C2 and C3, respectively, as compared to shell C1. The deformation response for shell C4 just before buckling, shown in Fig. 6c, exhibits a further reduction in the displacement gradients in the shell wall near the cutout, with an increase in the thickness of the reinforcement, as compared to shells C2 and C3. More specifically, the magnitude of the shell wall displacements range between -0.06 and 0.33 and correspond to a 91% reduction in the magnitude of the maximum inward displacement near the cutout as compared to shell C1. In addition, the maximum inward shell-wall displacement in shell C4 occurs just outside the reinforced region of the shell, and this response is unlike that of shells C1-C3 in which the maximum inward shell-wall displacement occurs at the free-edges of the cutout. Axial and circumferential traces illustrating the effects of the cutout reinforcement on the deformation response in shells C1 through C4 are compared in Figs. 7a and 7b, respectively. The regions of the shell that the trace data were taken from is marked by the dashed axial and circumferential lines superimposed on the displacement contour plot shown in Fig. 6a. The results show that the magnitude of the shell-wall displacements decrease near the cutout as the reinforcement thickness is increased, as expected. Furthermore, the results indicate that the character of the attenuation of the local displacements in shell C4 are somewhat different from those exhibited by shells C1 through C3. In particular, shell C4 exhibits additional waves in the displacement pattern along the length and around the circumference of the shell.

The character of the axial and circumferential stress resultant distributions just before buckling for shells C2 through C4 are similar to that of shell C1 shown in Fig. 4a. In particular, the shells exhibit regions of in-plane biaxial compression stress resultants near the cutout, however, the magnitudes of the stresses can be significantly different. More specifically, the magnitudes of the axial and circumferential stress resultant components in these regions of biaxial compression just before buckling are as follows: N_x = -580 lb/in and N_θ = -109 lb/in for shell C2, N_x = -615 lb/in and N_θ = -96 lb/in for shell C3, and N_x = -703 lb/in and N_θ = -87.5 lb/in for shell C4, as compared to N_x = -568 lb/in, and N_θ = -110 lb/in for shell C1. For comparison purposes, it is useful to define an axial stress concentration factor and a biaxial-stress ratio. The axial-stress concentration factor is defined as the local axial stress resultant value in the region of biaxial stress, N_x, normalized with respect to the far-field value of axial stress resultant $N_x^o = P/2\pi R$, where P is the axial load applied to the shell and R is the shell radius. The biaxial-stress ratio is defined as the ratio of local circumferential stress to axial stress in the region of biaxial compression, that is N_θ/N_x. The definitions of stress concentration factor and biaxial stress ratio are used herein unless otherwise specified. The stresses in the region of biaxial compression correspond to axial stress concentration factors equal to 1.20, 1.13, and 1.06, for shells C2, C3, and C4, respectively, as compared to 1.31 for shell C1, and biaxial stress ratios of 0.19, 0.16, and 0.12 for shells C2, C3, and C4, respectively, as compared to 0.19 for shell C1. These results indicate that the axial stress concentration factor and the biaxial-stress ratio decrease as the thickness of the cutout reinforcement increases.

The results indicate that the overall character of the local buckling response in shells C2-C4 is similar to that of shell C1. In particular, the local buckling responses in shells C2-C4 initiate near the cutouts and are caused by a nonlinear coupling between the localized regions of destabilizing in-plane biaxial compression stress resultants and the local shell-wall deformations. In addition, the locations at which buckling initiates in shells C2-C4 correspond to points within the reinforced region of the shells. However, the results also indicate that the character of the post-local-buckling response and the transient collapse response can be greatly affected by the reinforcement. For example, shell C2 exhibits a stable post-local-buckling response and global collapse response similar to that of shell C1. However, when the reinforcement thickness is increased, the shells no longer exhibit a stable post-local-buckling response; rather, the shell exhibits a global collapse, e.g., shells C3 and C4, and the shells collapse into a general instability mode-shape. The general instability mode shape for shell C3 is similar to that exhibited by shell C1 (see Fig. 3f), however, shell C4 buckles into a mode shape that consists of two half waves along the length of the shell and eight full waves around the circumference. Upon local buckling and global collapse, shells C2-C4 exhibit significant stress redistribution throughout the entire shell, similar to that exhibited by shell C1 as shown in Figs. 4b, and 4c.

Displacement contour patterns just before buck-

ling for shells C5-C7 (corresponding shells with 90°-ply cutout reinforcement) are shown in Figs. 8a-8c, respectively. The radial-displacement contour patterns for shells C5 through C7 indicate large-magnitude local deformations that rapidly attenuate away from the cutout, and are similar to the contours exhibited by shell C1 (see Fig. 3a). The magnitudes of the shell-wall deformations decrease as the thickness of the reinforcement increases, and the magnitude of the normalized displacements range from -0.58 to 0.35 for shell C5, -0.54 to 0.38 for shell C6, and -0.46 to 0.42 for shell C7, as compared to -0.65 to 0.4 for shell C1. These results correspond to a reduction in the magnitude of the local deformations by as much as 29% as the thickness of the reinforcement increases, as compared to shell C1. However, the reduction in the magnitude of the local displacements for these shells is significantly less than that exhibited by the corresponding shells with 0°-ply reinforcement which exhibited a maximum reduction of approximately 91%. In addition, axial and circumferential displacement traces illustrating the effects of the cutout reinforcement on the deformation response of shells C5 through C7 are compared in Figs. 9a and 9b, respectively. These results indicate that the thickness of the cutout reinforcement has a small effect on the magnitude and distribution of the shell wall deformations near the cutout. This behavior is in contrast to the significant variation in the deformation responses exhibited by the corresponding shells with 0°-ply reinforcement (shells C2 through C4) as shown in Figs. 7a and 7b.

The character of the axial and circumferential stress resultant distributions just before buckling for shells C5 through C7 are, for the most part, similar to that of shell C1 shown in Fig. 4a. However, the magnitudes of the stresses are significantly different. In particular, the magnitudes of the axial and circumferential stress resultant components in these regions of biaxial compression near the cutout just before buckling are as follows: N_x = -620 lb/in and N_θ = -103 lb/in for shell C5, N_x = -662 lb/in and N_θ = -94 lb/in for shell C6, and N_x = -759 lb/in and N_θ = -89 lb/in for shell C7, as compared to N_x = -568 lb/in, and N_θ = -110 lb/in for shell C1. These results correspond to axial-stress concentration factors equal to 1.25, 1.19, and 1.16, for shells C5, C6, and C7, respectively, as compared to 1.31 for shell C1 and biaxial-stress ratios of 0.17, 0.14, and 0.12 for shells C5, C6, and C7, respectively, as compared to 0.19 for shell C1. These results indicate that the axial-stress concentration factor and the biaxial-stress ratio decrease as the thickness of the cutout reinforcement increases. This trend is similar to the response trend exhibited by shells C2-C4. In addition, the results for these shells indicate that the magnitude of the axial-stress concentration factor and the biaxial stress ratio are, on average, 6.2% greater and 8.7% lower, respectively, as compared to the corresponding shells with 0°-ply reinforcement, shells C2-C4.

The results indicate that the overall character of the local buckling response in shells C5-C7 is similar to that of shell C1. In addition, the locations at which the buckling response initiates in the shells correspond to points within the reinforcement regions. However, the results also indicate that the character of the post-local-buckling response and the transient collapse response can be affected by reinforcement thickness. For example, shell C5 exhibits a similar stable post-local-buckling and global collapse responses as that of shell C1 and C2. However, as the reinforcement thickness is increased, the shell no longer exhibits a stable post-local-buckling response; rather, the local buckling response in the shell causes the global collapse of the shell to occur (e.g., shells C6 and C7). In addition, shells C5 and C6 exhibit post-collapse general instability mode shapes similar to that of shell C1. However, as the thickness of the reinforcement is increased, the shell exhibits a general instability mode shape that consists of two half waves along the length of the shell and eight full waves around the circumference of the shell. This mode shape is similar to the post-collapse mode shape exhibited by shell C4. Overall, these response trends are similar to those exhibited by the corresponding shells with 0°-ply cutout reinforcements, shells C2-C4. Upon local buckling and collapse, shells C5-C7 exhibit significant stress redistribution throughout the entire shell, similar to that exhibited by shell C1 that is shown in Figs. 4b, and 4c.

4.4-in. Square Reinforcement. Results for shells C8 through C13 are presented in this section. The cutout reinforcements for shells C8 through C10 consist of 4.4-in square-shaped 0° lamina plies and the cutout reinforcements for shells C11 through C13 consist of 4.4-in square-shaped 90° lamina plies. Shells C8 and C11 have 0.005-in-thick reinforcement, shells C9 and C12 have 0.01-in-thick reinforcement, and shells C10 and C13 have 0.02-in-thick reinforcement. Numerically predicted load-shortening response curves for shells C8 through C10 and shells C11 through C13, are presented in Figs. 10a and 10b, respectively. The quasi-static responses are indicated by the solid lines and the unstable, transient buckling responses are indicated by the dashed lines in the figure. The axial load P is normalized with respect to the bifurcation buckling load of the

corresponding shell without a cutout P_{cr} = 42,590 lbf, and the end-shortening Δ is normalized with respect to the shell length L. The local buckling points are marked with filled circles, and global collapse points are indicate by an **X**.

The results in Figs. 10a and 10b also show that the addition of reinforcement around the cutout can have a significant effect on the overall character of the response of the shell, and indicate similar trends to those shown by shells C2-C7 in Figs. 5a and 5b. In particular, the local buckling loads increase significantly as the thickness of the reinforcement increases. Specifically, the normalized buckling loads for shells C8, C9, and C10 are equal to 0.62, 0.73, and 0.84, respectively, as compared to the buckling load of 0.51 for the corresponding unreinforced shell C1. Similarly, the normalized buckling loads for shells C11, C12, and C13 are equal to 0.64, 0.76, and 0.92, respectively. The results also indicate that the shells with 90°-ply reinforcements considered here can exhibit significantly higher buckling loads than the corresponding shells with 0°-ply reinforcements, that is, the buckling loads for shells C11, C12, and C13 are 3.2, 4.1, and 9.5% higher than for shells C8, C9, and C10, respectively. In addition, the results indicate that the buckling loads of the shells increase as the reinforcement size increases. More specifically, the buckling loads for shells C8, C9, and C10 are 10, 18, and 12% higher than the buckling loads for the corresponding shells with 2.4-in square-shaped 0°-ply reinforcements, shells C2, C3, and C4, respectively. Similarly, the buckling loads for shells C14-C16 are 9, 18, and 29% higher than the corresponding buckling loads for shell with 2.4-in-square 90°-ply reinforcements C5, C6, and C7, respectively. Furthermore, the results indicate that some of the shells with thicker reinforcement, C9 through C13, no longer exhibit stable post-local-buckling responses. Rather, the local buckling response in each shell causes a disturbance of sufficient magnitude to cause the global collapse of the shell. This response characteristic is contrary to that of shell C8, which exhibits a stable post-local-buckling response before global collapse, similar to that exhibited by shell C1 (see Fig. 2a). Upon global collapse, each shell obtains a stable post-collapse configuration, accompanied by a significant reduction in axial load-carrying capability. The normalized post-collapse load levels range from 0.31 to 0.35 and these post-collapse load levels are similar to those exhibited by the corresponding shells with smaller reinforcement; that is, shells C2-C7 (see Figs. 5a and 5b).

Displacement contour patterns just before buckling for shells C8-C10 are shown in Figs. 11a-11c, respectively. The radial displacements w are normalized with respect to the shell-wall thickness t = 0.04 in. The outer boundary of the cutout reinforcement in each shell is marked in the figures with solid lines. In general, the results indicate that the character of the deformation patterns just before local buckling can change significantly as the thickness of the reinforcement increases. In addition, the magnitude of the local deformations near the cutout decreases as the thickness of the reinforcement increases. In particular, the displacement contour patterns exhibited by shell C8, shown in Fig. 11a, exhibit a large-magnitude local deformation response that rapidly attenuates away from the cutout in a manner that is similar to that of shell C1. The magnitude of the normalized shell wall deformations range between -0.47 to 0.35 for shell C8, as compared to -0.65 to 0.4 for shell C1, and correspond to as much as 28% reduction in the magnitude of the local deformations near the cutout, as compared to shell C1. However, the character and the magnitude of the local deformations change significantly as the thickness of the reinforcement increases. In particular, the magnitude and character of the displacement gradients near the cutout in shell C9 just before buckling are similar to the displacement gradients exhibited by shell C8. However, the magnitude of the deformations away from the cutout and the attenuation lengths of these deformations increase as the thickness of the reinforcement increases, as shown in Figs. 11b, 12a, and 12b. Furthermore, the results indicate that the displacement gradients near the cutout are reduced significantly as the thickness of the cutout reinforcement is increased further and exhibit normalized displacement magnitudes that range from 0.37 to 0.57; e.g., see shell C10 shown in Fig. 11c. In addition, the large-magnitude displacements away from the cutout, and the attenuation length of these displacements increase, and the shell exhibits normalized displacement values as large as -0.40, as shown in Figs. 11c, 12a, and 12b. Overall, these results indicate that the local deformations near the cutout decrease with an increase in the thickness of the cutout reinforcement. However, the shells also exhibit increasing large-magnitude deformations away from the cutout and the attenuation length of these deformations increases as the thickness of the reinforcement is increased. This response trend is similar to that exhibited by the corresponding shells with the smaller 2.4-in-square reinforcement, however, the magnitudes of the deformations away from the cutout are as much as four times larger. Additionally, the attenuation lengths are approximately twice as long in shells C8-C10, as those exhibited by the corresponding shells with the smaller 2.4-in-square reinforcement.

The character of the local axial and circumferential stress resultant distributions just before buckling for

shells C8 through C10 are, largely, similar to those predicted for shell C1 shown in Fig. 4a. However, the magnitudes of the stress resultants can vary significantly as the thickness of the cutout reinforcement increases. In particular, the magnitudes of the axial and circumferential stress resultant components in these regions of biaxial compression just before buckling are N_x = -719 lb/in and N_θ = -129 lb/in for shell C8, and N_x = -865 lb/in and N_θ = -126 lb/in for shell C9 (N_x = -568 lb/in, and N_θ = -110 lb/in for shell C1). These results correspond to axial-stress concentration factors equal to 1.36 and 1.40 for shells C8 and C9, respectively, as compared to 1.31 for shell C1 and biaxial-stress ratios of 0.18 and 0.15 for shells C8 and C9, respectively, and 0.19 for shell C1. In addition, the magnitude of the axial-stress concentration factor and the biaxial stress ratio for shells C8-C10 are, 22, 5, and 5.7% greater on average than those exhibited by the corresponding shells with the smaller sized cutout reinforcement, C2-C4, respectively. In contrast, the axial and circumferential stress resultant distributions change significantly as the thickness of the reinforcement increases further. Specifically, shell C10 exhibits localized regions of in-plane biaxial compression stress resultants in the bending boundary layer region of the shell and the magnitudes of the stress are N_x = -985 lb/in and N_θ = -58 lb/in. These stress resultants correspond to an axial-stress concentration factor of 1.38, and a biaxial-stress ratio of 0.06.

The deformation patterns and stresses indicate that the initiation of the local buckling response of shells C8 and C9 is similar to that of shell C1. However, the results also indicate that the character of the post-local-buckling response and the transient collapse response can be greatly affected by the cutout reinforcement. In particular, shell C8 exhibits a similar stable post-local buckling response and global collapse response as that exhibited by shell C1 as shown in Figs. 3c-3f. However, as the thickness of the reinforcement increases the shell no longer exhibits a stable post-local-buckling response. Instead, the local response in shell causes the overall global collapse to occur (e.g., shell C9). This response trend for shells C8 and C9 is similar to that exhibited by the corresponding shells with smaller reinforcement, shells C2 and C3. As the thickness of the reinforcement is increased further, the shell no longer exhibits a local buckling response near the cutout. For this case, a local buckling response initiates in the bending boundary layer region where large-magnitude inward deformations occur, e.g., see shell C10, and Fig. 11c). These deformations couple with localized destabilizing in-plane biaxial compression stress resultants in the bending boundary layer region of the shell. This localized buckling response in the bending boundary region of the shell causes the global collapse of the shell. This response characteristic is unlike that of the corresponding shell with the smaller, 2.4-in-square cutout reinforcement (shell C4) which exhibits local buckling near the cutout. This result illustrates how the reinforcement size can have a significant effect on the character of the buckling response of the shell. In particular, the cutout reinforcement has suppressed the local buckling response near the cutout and the shell now exhibits a different localized response in the bending boundary region that causes the buckling of the shell. Upon local buckling and collapse, shells C8-C10 exhibit significant stress redistribution throughout the entire shell in a manner similar to that of shell C1 that is shown in Figs. 4b, and 4c.

The deformation response just before buckling for shells C11-C13 (corresponding shells with 90°-ply cutout reinforcement) are shown in Figs. 13a-13c, respectively and also illustrate how the thickness of the reinforcement can have a significant effect on the deformation response. In particular, the radial-displacement contour patterns of shells C11 and C12 show similar local large-magnitude deformations that rapidly attenuate away from the cutout and are similar to those exhibited by shell C1. However, as the thickness of the reinforcement increases, the shell exhibits significant differences in the deformation pattern (e.g., shell C13), as compared to shells C11 and C12. Specifically, large-magnitude radial deformations develop in a large portion of the shell away from the cutout and include two large inward buckles that develop in the bending boundary layer region of the shell. In addition, the magnitudes of the shell wall deformations increase as the thickness of the reinforcement increases from 0.005 inches to 0.01 inches; that is, the magnitudes of the shell-wall deformations range between -0.67 to 0.39 for shell C11 and between -0.96 to 0.68 for shell C12, as compared to -0.65 to 0.4 for shell C1. These results correspond to an increase in the magnitude of the displacements by as much as 70% in shells C11 and C12. However, upon further increase of the reinforcement thickness to 0.02 inches, the magnitude of the normalized shell-wall deformations decrease significantly to between -0.37 to 0.45 for shell C13, and correspond to a 43% decrease in the magnitude of the deformations, as compared to shell C1. Axial and circumferential traces illustrating the effects of the cutout reinforcement on the deformation response of shells C11 through C13 are compared in Figs. 14a and 14b, respectively. The results show that significant changes in the character of the deformation response of the shells occur as the thickness of the reinforcement is changed. In particular, shell C13 ex-

hibits a significant increase in the attenuation length of the local deformation response as compared to shells C11 and C12. These results indicate that, for the most part, the character and magnitudes of the deformation responses for shells with 4.4-in-square 90°-ply reinforcement (see shells C11 through C13 shown in Figs. 11a-11c) can be significantly different from the corresponding shells with 0°-ply reinforcement (see shells C8 through C10 in Figs. 13a-13c). In particular, the reinforcement in shells C8-C10 reduces the local deformations near the cutout just before buckling. In contrast, shells C11-C13 can exhibit increases in the local deformations with an increase in the reinforcement thickness.

The character of the local axial and circumferential stress resultant distributions near the cutout just before buckling for shells C11 through C13 are, for the most part, similar to that of shell C1 shown in Fig. 4a. However, the magnitudes of the stress resultants can be significantly different. In particular, the magnitudes of the axial and circumferential stress resultant components in these regions of biaxial compression near the cutout just before buckling are as follows: N_x = -681 lb/in and N_θ = -126 lb/in for shell C11, and N_x = -843 lb/in and N_θ = -173 lb/in for shell C12, as compared to N_x = -568 lb/in, and N_θ = -110 lb/in for shell C1. These results correspond to axial-stress concentration factors equal to 1.26 and 1.30 (1.31 for shell C1) and biaxial-stress ratios of 0.19 and 0.21, for shells C11 and C12, respectively (0.19 for shell C1). These results indicate that the axial-stress concentration factor and the biaxial stress ratio increase as the thickness of the cutout reinforcement increases. The magnitude of the axial-stress concentration factor and the biaxial-stress ratio for these shells are, on average, approximately 7.2% lower and 21% greater, respectively, as compared to the corresponding shells with 0°-ply reinforcement (shells C8-C9). This trend exhibited by the shells with 4.4-in-square reinforcements is contrary to that of the shells with smaller 2.4-in-square cutout reinforcements, in which the shells with 0°-ply reinforcement exhibited larger-magnitude axial-stress concentration factors and lower biaxial-stress ratios than that of the corresponding shells with 90° reinforcement. In addition, the results indicate that the magnitude of the stress concentration factors and the biaxial-stress ratios are, on average, 0.8 and 39.9% greater than those exhibited by the corresponding shells with the smaller reinforcement, shells C5-C7. In contrast, the axial and circumferential stress resultant distributions change significantly as the thickness of the reinforcement increases further to 0.02 inches. Specifically, shell C13 exhibits localized regions of in-plane biaxial compression stress resultants in the bending boundary layer region of the shell and the magnitudes of the stress resultants are N_x = -838 lb/in, and N_θ = -128 lb/in, which correspond to an axial-stress concentration factor of 1.08, and a biaxial-stress ratio of 0.15. This response characteristic is similar to that of shell C10. The results also indicate that shells C11-C13 exhibit similar post-local-buckling and collapse response trends as those exhibited by the corresponding shells with 0°-ply reinforcement, shell C8-C10.

8.0-in. Square Reinforcement. Results for shells C14 through C19 are presented in this section. The cutout reinforcements for shells C14 through C16 consist of 8.0-in by 8.0-in square-shaped 0° lamina plies and the cutout reinforcements for shell C17 through C19 consist of 8.0-in by 8.0-in square-shaped 90° lamina plies. Shells C14 and C17 have 0.005-in-thick reinforcement, shells C15 and C18 have 0.01-in-thick reinforcement, and shells C16 and C19 have 0.02-in-thick reinforcement. Predicted load-shortening response curves for shells C14 through C16 and shells C17 through C19, are presented in Figs. 15a and 15b, respectively. The quasi-static responses are indicated by solid lines and the unstable, transient buckling responses are indicated by dashed lines in the figure. The axial load P is again normalized with respect to the bifurcation buckling load of the corresponding shell without a cutout obtained from a linear eigenvalue analysis P_{cr} = 42,590 lbf, and the end-shortening displacement Δ is normalized with respect to the shell length L. The local buckling points are marked with filled circles, and global collapse points are indicated by an **X**. These results show that the addition of reinforcement around the cutout can have a significant effect on the overall character of the response of the shell, and exhibit, for the most part, similar response trends to those shown by shells C2-C7 in Figs. 5a and 5b, and shells C8-C13 in Figs. 10a and 10b. In particular, the local buckling loads of the shells increase as the thickness of the reinforcement increases; that is, the normalized buckling loads for shells C14, C15, and C16 are equal to 0.61, 0.72, and 0.74, respectively, as compared to the normalized buckling load of 0.51 for the corresponding unreinforced shell C1. However, the results indicate that an increase in the size of the cutout reinforcement in shells C14-C16 causes a 1.6, 1.4, and 12% reduction in the buckling loads as compared to the corresponding buckling loads for shells C8-C10 (shells with 4.4-in-square 0°-ply reinforcements), respectively. Furthermore, the result indicate that the effective axial compression stiff-

ness of the shell increases as the thickness of the reinforcement increases, as shown in Fig. 15a. This result is in contrast to the results from shells C2-C4 and C8-C10 which exhibit negligible changes in the effective axial stiffness of the shells with the addition of the cutout reinforcements. The normalized buckling loads for shells C17, C18, and C19 equal 0.66, 0.83, and 0.93, respectively, and correspond to a 3.1, 9.2, and 1% increase in the buckling load over the corresponding buckling loads for shells C11, C12, and C13 (shells with 4.4-in-square 90^{o}-ply reinforcements), respectively. The results indicate that the shells with 90^{o}-ply reinforcements considered herein exhibit significantly higher buckling loads than the corresponding shells with 0^{o}-ply reinforcements; that is, the buckling loads for shells C17, C18, and C19 are 8.2, 15.3, and 25.7% higher than the buckling loads of shells C14, C15, and C16, respectively. This response trend is similar to that exhibited by shells C8-C13, however, the differences in the buckling loads are significantly greater for the shells with the 8.0-in-square reinforcement. Furthermore, the results indicate that some shells with thicker cutout reinforcement no longer exhibit stable post-local-buckling responses. Rather, the local buckling response in each shell causes a disturbance in the shell of sufficient magnitude to cause the global collapse of the shell, e.g., shells C15 through C19. In contrast, shell C14 which exhibits a stable post-local-buckling response before global collapse similar to that exhibited by shell C1 (see Fig. 2a). Upon global collapse, each shell obtains a stable post-collapse configuration and exhibits a significant reduction in axial load carrying capability. The normalized post-collapse load levels for shells C14-C19 range from 0.34 to 0.39 and are as much as 26% greater than the corresponding post-collapse load-levels of shells C2-C7 and C8-C13.

Displacement contour patterns just before buckling for shells C14-C16 are shown in Figs. 16a-16c, respectively. The radial displacements w are normalized with respect to the shell-wall thickness t = 0.04 in. The outer boundary of the cutout reinforcement in each shell is marked in the figures with solid lines. These results also indicate that the character of the deformation response in the shell just before buckling changes significantly as the thickness of the reinforcement increases. For example, the displacement contour patterns exhibited by shells C14 and C15 shown in Figs. 16a and 16b, respectively, exhibit similar local large-magnitude deformations that rapidly attenuate away from the cutout and are similar to the response exhibited by shell C1. In addition, the magnitudes of the normalized shell-wall deformations increase as the thickness of the reinforcement increases and range between -0.54 to 0.48 for shell C14 and between -0.98 to 0.62 for shell C15, and correspond to as much as a 20% and 50.8% increase in the magnitude of the local deformations near the cutout, respectively, as compared to shell C1. In contrast, the character of deformation response just before buckling for shell C16, changes significantly with an increase in the thickness of the reinforcement as shown in Fig. 16c, as compared to shells C14 and C15. In particular, the local deformation response near the cutout is characterized by a large ellipse-shaped inward buckle and the semi-major axis of the buckle is aligned with the longitudinal axis of the shell. In addition, large-magnitude outward radial deformations occur on either side of the cutout. Furthermore, the displacement gradients near the cutout in shell C16 are reduced significantly with normalized displacement magnitudes that range from -0.30 to 0.47, e.g., see Figs. 17a and 17b, and correspond to a 27% reduction in the local displacement gradient. Generally, the results indicate that the magnitude of the shell-wall displacements away from the cutout and the attenuation length of these shell wall displacements increase as the thickness of the reinforcement increases, as shown in Figs. 17a and 17b, respectively. Furthermore, the magnitude of the deformations and the attenuation length of these deformations are significantly larger than those exhibited by the corresponding shells with 2.4-in- and 4.4-in-square cutout reinforcement.

The character of the local axial and circumferential stress resultant distributions near the cutout just before buckling for shells C14 through C16 are, for the most part, similar to those of shell C1 (shown in Fig. 4a). However, the magnitudes of the stress resultants can vary significantly as the thickness of the reinforcement increases. The magnitudes of the axial and circumferential stress resultant components in the regions of bi-axial compression just before buckling are N_x = -719 lb/in and N_θ = -121 lb/in for shell C14, and N_x = -940 lb/in and N_θ = -227 lb/in for shell C15. The results correspond to axial-stress concentration factors equal to 1.39, 1.55, for shells C14, C15, respectively, (1.31 for shell C1) and biaxial-stress ratios of 0.17, 0.24, for shells C14, C15, respectively, (0.19 for shell C1). The stress concentration factors for these shells are, on average, 26.2 and 6.5% greater than those exhibited by the corresponding shells with 2.4-in- and 4.4-in-square reinforcements, respectively. Similarly, the results indicate that biaxial-stress ratios for these shells are, on average, 20.0 and 27.3% greater than those exhibited by the corresponding shells with 2.4-in- and 4.4-in-square reinforcements, respectively. In contrast, shell C16 developed regions of biaxial stress resultants in the bending boundary region of the shell with stress resultant values of N_x = -867 lb/in, and N_θ = -163 lb/in for shell

C16, and correspond to an axial-stress concentration factor of 1.38 and a biaxial-stress ratio of 0.16. This response characteristic is similar to that exhibited by the corresponding shell with 4.4-in-square reinforcement, shell C10. The results indicate that the initiation of the local buckling response of shells C14 and C15 is similar to that of shell C1, however, the results also indicate that the character of the post-local-buckling response and the transient collapse response can be effected by the reinforcement. For example, shell C14 exhibits a similar stable post-local-buckling response and global collapse response as that of shell C1. As the thickness of the reinforcement increases, the shell no longer exhibits a stable post-local-buckling response. Rather, the local buckling response in the shell causes the overall collapse of the shell (e.g., shell C15). As the thickness of the reinforcement is increased further, the shell no longer exhibits a local buckling response near the cutout, rather, a local buckling response initiates in the bending boundary layer region of the shell similar to that exhibited by shell C10. This localized buckling response in the bending boundary layer region of the shell initiates the global collapse of the shell. This response trend associated with the post-local-buckling and global collapse response is similar to that exhibited by the corresponding shells with 4.4-in-square reinforcement.

Displacement contour patterns just before buckling for shells C17-C19 (corresponding shells with 90°-ply cutout reinforcement) are shown in Figs. 18a-18c, respectively, and indicate that the cutout reinforcement can have a significant effect on the deformation response in the shell. In particular, the radial displacement contour patterns exhibited by shells C17 and C18 indicate local large-magnitude deformations similar to those for the corresponding 0°-ply reinforced shells C14 and C15 and the unreinforced shell C1. The magnitudes of the shell-wall deformations range from -0.8 to 0.41 for shell C17 and -0.71 to 0.45 for shell C18, and indicate that the magnitude of the local deformations increase by as much as 23 and 9.2% in shells C17, C18, respectively, as compared to shell C1. However, as the thickness of the reinforcement increases further, the shell exhibits a significant reduction in the local deformations (e.g., shell C19). In addition, large-magnitude radial deformations develop in a large portion of the shell away from the cutout and include four large inward ellipse-shaped buckles that develop in the bending boundary layer region of the shell and is a similar deformation response to that of shell C16 (e.g., Fig. 16c). The magnitude of the shell-wall deformations ranges from -0.37 to 0.36 and correspond to a 43% increase in the deformations away from the cutout. Axial and circumferential traces illustrating the effects of the cutout reinforcement on the deformation response of shells C17 through C19 are compared in Figs. 19a and 19b, respectively. The results show the significant changes in the character of the deformation response of the shells as the thickness of the reinforcement is changed. In particular, shell C19 exhibits a slight increase in the magnitude of the shell-wall deformations away from the cutout and an increase in the attenuation length of the local deformation response around the circumference of the shell as compared to shells C17 and C18. These results indicate that, for the most part, the character of the deformation responses for shells with 8.0-in-square 90°-ply reinforcement (e.g., see shells C17 through C19 Figs. 18a-18c), is somewhat similar to that of the corresponding shells with 0°-ply reinforcement (e.g., see shells C14 through C16 in Figs. 16a-16c). However, the magnitudes and attenuation lengths of the deformations in shells C17-C19 are generally smaller then those of shells C14-C16. In addition, the magnitude of the deformations in shells with 8.0-in-square reinforcement can be as much as 38% larger than those of the corresponding shells with 2.4-in-square reinforcement, and 26% smaller than those exhibited by the corresponding shells with 4.4-in-square reinforcement.

The character of the local axial and circumferential stress resultant distributions just before buckling for shells C17 through C19 are, for the most part, similar to that of shell C1 (shown in Fig. 4a). However, the magnitudes of the stress resultants can be significantly different as the thickness of the reinforcement increases. In particular, the axial and circumferential stress resultant components in these regions of biaxial compression just before buckling are N_x = -736 lb/in and N_θ = -156 lb/in for shell C17, and N_x = -888 lb/in and N_θ = -145 lb/in for shell C18. These results correspond to axial-stress concentration factors equal to 1.32 and1.27 for shells C17 and C18, respectively, (1.31 for shell C1) and biaxial-stress ratios of 0.21 and 0.16, for shells C17 and C18, respectively (0.19 for shell C1). These results indicate that the axial-stress concentration factor and the biaxial-stress ratio decrease as the thickness of the cutout reinforcement increases. In addition, the results indicate that the magnitude of the axial-stress concentration factors for these shells is, on average, 1.9% lower and the biaxial-stress ratio is, on average, 9.8% lower than those exhibited by the corresponding shells with 0°-ply reinforcement. Furthermore, the results indicate that the stress concentration factors are, on average, 0.8 and 1.7% greater than the corresponding shells with 2.4-in-, and 4.4-in-square reinforcements, respectively. Similarly, the results indicate that the biaxial-stress ratios are, on average, 30.6% greater and 10.5% less than the corresponding shells with 2.4-in-, and 4.4-in-square

reinforcements, respectively. However, as the thickness of the reinforcement increases further, the shell exhibits regions of biaxial compression stress resultants in the bending boundary layer region of the shell similar to that exhibited by shell C16 and the stress resultants are N_x = -865 lb/in and N_θ = -96 lb/in and correspond to a stress concentration factor of 1.09 and a biaxial-stress ratio of 0.11. In general, the results indicate that shells C17-C19 exhibit similar post-local-buckling and collapse response trends as those exhibited by the corresponding shells with 0°-ply reinforcement, shell C14-C16.

Response Trends and Design Considerations

The results presented herein illustrate how a compression-loaded composite shell with an unreinforced cutout can exhibit a complex nonlinear response, and that the character of the response can be significantly affected by the addition of reinforcement around the cutout. The buckling response in the shell is caused by a complex nonlinear coupling between local shell-wall deformations and in-plane destabilizing compression stresses near the cutout. The cutout reinforcement can retard the onset of buckling by retarding the onset of the local deformations and stress concentrations in the shell near the cutout. The results presented herein indicate that, for the most part, as the thickness and the size of the cutout reinforcement increases, the buckling load of the shell increases, as expected. In addition, the results show that reinforcement orientation can have a very pronounced effect on the shell response. In particular, shells with 90°-ply cutout reinforcement have higher buckling loads than the corresponding shells with 0° cutout reinforcement. Furthermore, shells with 0°-ply reinforcement exhibit smaller-magnitude deformations near the cutout than the corresponding shells with 90°-ply reinforcement. However, the shells with 0°-ply reinforcement can exhibit larger-magnitude deformations away from the cutout, as compared to the corresponding shells with 90° reinforcement. In particular, as the size and thickness of the reinforcement increases, the magnitude and attenuation length of the deformations away from the cutout increases. These changes in character of the deformation response can be important in understanding the formation of local bending gradients in thin-walled laminated shells. In particular, large-magnitude bending gradients in thin-walled laminated shells have been shown to cause interlaminar material failures (e.g., see Ref. 7). The results also indicate that, in general, shells with 1 or 2-ply reinforcement, i.e., 0.005-in- and 0.01-in-thick reinforcement, exhibit local buckling near the cutout. The local buckling of the shell is caused by a complex nonlinear coupling between local shell-wall deformations and in-plane destabilizing compression stresses near the cutout, and this response is similar to that exhibited by the corresponding shell with an unreinforced cutout, C1. In contrast, some shells with 4-ply reinforcements no longer exhibit local buckling near the cutout. Rather, the shells exhibit local buckling in the bending boundary layer region near the ends of the shell. For these cases, localized destabilizing in-plane biaxial stresess form in the bending boundary region of the shell and these stresses couple with the bending boundary layer deformations to cause local buckling to initiate in the bending boundary layer region of the shell. The results also indicate that shells with 1-ply reinforcement tend to exhibit stable post-local-buckling responses and can support additional load before global collapse. In contrast, the local buckling response of shells with thicker reinforcement (2-, and 4-ply-thick) can cause the overall global collapse of the shells. The results also indicate that shells with thinner reinforcements exhibit post-collapse general instability mode-shapes similar to that of the corresponding shell with an unreinforced cutout and are characterized by one half wave along the length of the shell and eight full waves around the circumference. In contrast, shells with thicker reinforcement can exhibit a post-collapse general instability mode-shapes that consists of two half waves along the length and eight full waves around the circumference.

The results indicate that shells with reinforced cutouts exhibit local stress distributions near the cutout similar to that exhibited by the corresponding shell with an unreinforced cutout. In particular, the shells exhibit significant axial and circumferential stress concentrations near the cutout and regions of in-plane biaxial compression stress. However, the magnitudes of the stress concentrations and the biaxial-stress ratio just before buckling can vary significantly as the reinforcement orientation, size, and thickness vary. In particular, shells with 2.4-in-square cutout reinforcements exhibit axial-stress concentration factors that are, on average, 11% lower than the corresponding shell with an unreinforced cutout. Similarly, these shells exhibit biaxial-stress ratios that are, on average, 25% greater than that of the shell with an unreinforced cutout. In addition, there is at most a 5% difference in the stress concentration factors and the biaxial-stress ratios exhibited by shells C2-C7. As the reinforcement size increase, the axial-stress concentration factors and the biaxial-stress ratios increase significantly for shells with 0°-ply reinforcements and the stress concentration factor and the biaxial-stress ratio are, on average, 12.2% and 70.8% greater than that of the unreinforced shell C1, respec-

tively. Similarly, shells with 90°-ply reinforcement exhibit biaxial-stress ratios that are, on average, 54% greater than that of the shell with an unreinforced cutout. However, the axial-stress concentration factors remain, on average, 1.1% lower than that exhibited by the unreinforced shell. These results suggest that shells with the 90°-ply reinforcement continue to achieve higher buckling loads as the reinforcement size increases, as compared to the corresponding shells with 0°-ply reinforcement, because the shells with 90°-ply reinforcement do not generate increasingly larger magnitudes of axial-stress concentrations as the reinforcement size increases. In contrast, shells with 0°-ply reinforcement exhibit significant increases in the magnitude of the radial deformations and the axial-stress concentrations near the cutout at lower applied load levels.

For the most part, the response trends for the shells presented herein are consistent with what one might expect, however, the shells with 8.0-in-square 0°-ply cutout reinforcement, C14-C16, exhibited some unexpected behavioral characteristics. In particular, these shells exhibited lower buckling loads than those exhibited by the corresponding shells with smaller 4.4-in-square reinforcements. Most notably, shell C16, with a 4-ply-thick reinforcement, exhibited a normalized buckling load of 0.74 as compared to 0.84 for the corresponding shell with a 4.4-in square cutout reinforcement, shell C10. Furthermore, these shells exhibit substantially larger magnitudes of radial deformations and larger magnitudes of stress concentrations and biaxial-stress ratios near the cutout than those exhibited by corresponding shells with smaller-size reinforcements. The results indicate that the load in the shell is redistributed into the region of the shell near the reinforcement and causes the higher magnitude destabilizing stresses and deformations to occur in the bending boundary layer region of the shell at lower applied load levels and ultimately cause the buckling of these shells to occur at lower applied load levels. In addition, these shells exhibit buckling loads that are significantly lower than the corresponding linear bifurcation buckling loads. In particular, the predicted buckling load for shell C16 is 12.6% lower than the corresponding bifurcation buckling load.

Concluding Remarks

The results from a numerical study of the response of thin-wall compression-loaded quasi-isotropic laminated composite cylindrical shells with reinforced and unreinforced square cutouts have been presented. The results identify some of the effects of cutout-reinforcement orthotropy, size, and thickness on the nonlinear response of the shells. A high-fidelity nonlinear analysis procedure has been used to predict the nonlinear response of the shells.

The results presented herein indicate that a compression-loaded shell with an unreinforced cutout can exhibit a complex nonlinear response that is not typically found in the corresponding shell without a cutout. In particular, a local buckling response occurs in the shell that is caused by a localized nonlinear coupling between local shell-wall deformations and in-plane destabilizing compression stresses near the cutout. In general, the addition of reinforcement around a cutout in a compression-loaded shell can have a significant effect on the shell response, as expected. In particular, results have been presented that indicate that the reinforcement can affect the local deformations and stresses near the cutout so as to retard or suppress the onset of local buckling in the shell near the cutout. For some cases, the local buckling response in the shell results in a stable postbuckling response near the cutout and additional load can be applied to the shell before it undergoes a global collapse. For other cases, the local response in the shell causes a disturbance of sufficient magnitude in the shell to cause global collapse to occur immediately after the local instability occurs. For still other cases, the reinforcement suppresses the local buckling response near the cutout and causes buckling to occur in the bending boundary region of the shell. For the most part, the buckling load of the shell increases as the size and thickness of the cutout reinforcement increases. However, some results indicate that shells with a larger 0°-ply reinforcement can actually exhibit an increase in the magnitude of local deformations and stresses in the shell, and cause a reduction in the buckling load as compared to the corresponding shell with a smaller reinforcement. For these cases, the results indicate that this reinforcement configuration causes a redistribution of the loads into the reinforced region of the shell; causes larger-magnitude displacements and stresses to occur at lower applied-load levels in the shell; hence, causes the buckling of the shell at lower applied load levels. The results indicate that shells with 90°-ply cutout reinforcement tend exhibit higher buckling loads than the corresponding shells with 0°-ply reinforcement. The results suggest that shells with the 90°-ply reinforcement continue to achieve higher buckling loads because the shells with 90°-ply reinforcement exhibit smaller-magnitude axial-stress concentrations. In contrast, shells with 0°-ply reinforcement exhibit larger-magnitude axial-stress concentrations near the cutout.

Overall, the results suggest that tailoring the

orthotropy, thickness and size of a cutout reinforcement in a compression-loaded shell can result in significant increases in the buckling load, and can reduce the local deformations and stresses near the cutout. However, the results also suggest that a nonlinear analysis may be necessary to accurately characterize the complex nonlinear behavior exhibited by these structures. A modern high-fidelity nonlinear analysis procedure was used in the study and offers the opportunity to provide insight into the effects of various cutout reinforcement concepts on the response of compression-loaded shell structures. Moreover, results from a high-fidelity analysis procedure can improve some of the engineering approximations and methods that are used in the design of reinforced cutouts in shell structures.

References

1. Lur'e, A. I., "Statics of Thin-walled Elastic Shells," State Publishing House of Technical and Theoretical Literature, Moscow, 1947; translation, AEC-tr-3798, Atomic Energy Commission, 1959.

2. Lekkerkerker, J. G., "On the Stress Distribution in Cylindrical Shells Weakened by a Circular Hole," Ph.D. dissertation, Technological University, Delft, The Netherlands, 1965.

3. Brogan, F. A. and Almroth, B. O., "Buckling of Cylinders with Cutouts," *AIAA Journal*, Vol. 8, No. 2, February 1970, pp. 236-240.

4. Tennyson, R. C., "The Effects of Unreinforced Circular Cutouts on the Buckling of Circular Cylindrical Shells," *Journal of Engineering for Industry*, Transactions of the American Society of Mechanical Engineers, Vol. 90, November 1968, pp. 541-546.

5. Starnes, J. H., "The Effect of a Circular Hole on the Buckling of Cylindrical Shells," Ph. D. dissertation, California Institute of Technology, Pasadena, California, 1970.

6. Hilburger, M. W., Starnes, J. H., Jr., and Waas, A. M. "A Numerical and Experimental Study of the Response of Selected Compression-loaded Composite Shells with Cutouts," *Proceedings of the 39th AIAA/ASME/ASCE/AHS/ASC Structures, Structural Dynamics, and Materials Conference*, Long Beach, CA. AIAA Paper No. 98-1768, 1998.

7. Starnes, J. H., Jr., Hilburger, M. W., and Nemeth, M. P., "The Effects of Initial Imperfections on the Buckling of Composite Shells," *Composite Structures: Theory and Practice*, ASTM STP 1383, P. Grant and C. Q. Rousseau, Eds., American Society for Testing and Materials, 2000, pp. 529-550.

8. Almroth, B. O. and Holmes, A. M. C., "Buckling of Shells with Cutouts, Experiment and Analysis," *International Journal of Solids and Structures*, Vol. 8, August 1972, pp.1057-1071.

9. Cervantes, J. A. and Palazotto, A. N., "Cutout Reinforcement of Stiffened Cylindrical Shells," *Journal of Aircraft*, Vol. 16, March 1979, pp. 203-208.

10. Toda, S, "Buckling of Cylinders with Cutouts Under Axial Compression," *Experimental Mechanics*, pp. 414-417, December 1983.

11. Kuhn, P., *Stresses in Aircraft and Shell Structures*, Mcgraw-Hill Book Company, New York, 1956.

12. Hilburger, M. H., and Starnes, J. H., Jr., "High-fidelity Analysis of Compression-loaded Composite Shells," *Proceedings of the 42st AIAA/ASME/ASCE/AHS/ASC Structures, Structural Dynamics, and Materials Conference*, Seattle, WA. AIAA Paper No. 2001-1394, 2001.

13. Rankin, C. C., Brogan, F. A., Loden, W. A., and Cabiness, H. D., "STAGS Users Manual, Version 4.0," Lockheed Martin Missiles & Space Co., Inc., Advanced Technology Center, Report LMSC P032594, 1999.

14. Riks, E., "Progress in Collapse Analysis," *Journal of Pressure Vessel Technology*, Vol. 109, pp. 27-41, 1987.

15. Park, K. C., "An Improved Stiffly Stable Method for Direct Integration of Nonlinear Structural Dynamics," *Journal of Applied Mechanics*, Vol. 42, pp. 464-470, June 1975.

16. Riks, E., Rankin, C. C., and Brogan, F. A., "On the Solution of Mode Jumping Phenomena in Thin-walled Shell Structures," *Computer Methods in Applied Mechanics and Engineering*, Vol. 136 (1-2), pp. 59-92, 1996.

Table 1. Shell Identification Codes and Reinforcement Configuration

Shell Identification Code	Reinforcement Size, in. x in.	Reinforcement Ply Orientation, deg.	Reinforcement thickness, in. (# of plies)
C1	-	-	-
C2	2.4 x 2.4	0	.005 (1)
C3	2.4 x 2.4	0	.01 (2)
C4	2.4 x 2.4	0	.02 (4)
C5	2.4 x 2.4	90	.005 (1)
C6	2.4 x 2.4	90	.01 (2)
C7	2.4 x 2.4	90	.02 (4)
C8	4.4 x 4.4	0	.005 (1)
C9	4.4 x 4.4	0	.01 (2)
C10	4.4 x 4.4	0	.02 (4)
C11	4.4 x 4.4	90	.005 (1)
C12	4.4 x 4.4	90	.01 (2)
C13	4.4 x 4.4	90	.02 (4)
C14	8.0 x 8.0	0	.005 (1)
C15	8.0 x 8.0	0	.01 (2)
C16	8.0 x 8.0	0	.02 (4)
C17	8.0 x 8.0	90	.005 (1)
C18	8.0 x 8.0	90	.01 (2)
C19	8.0 x 8.0	90	.02 (4)

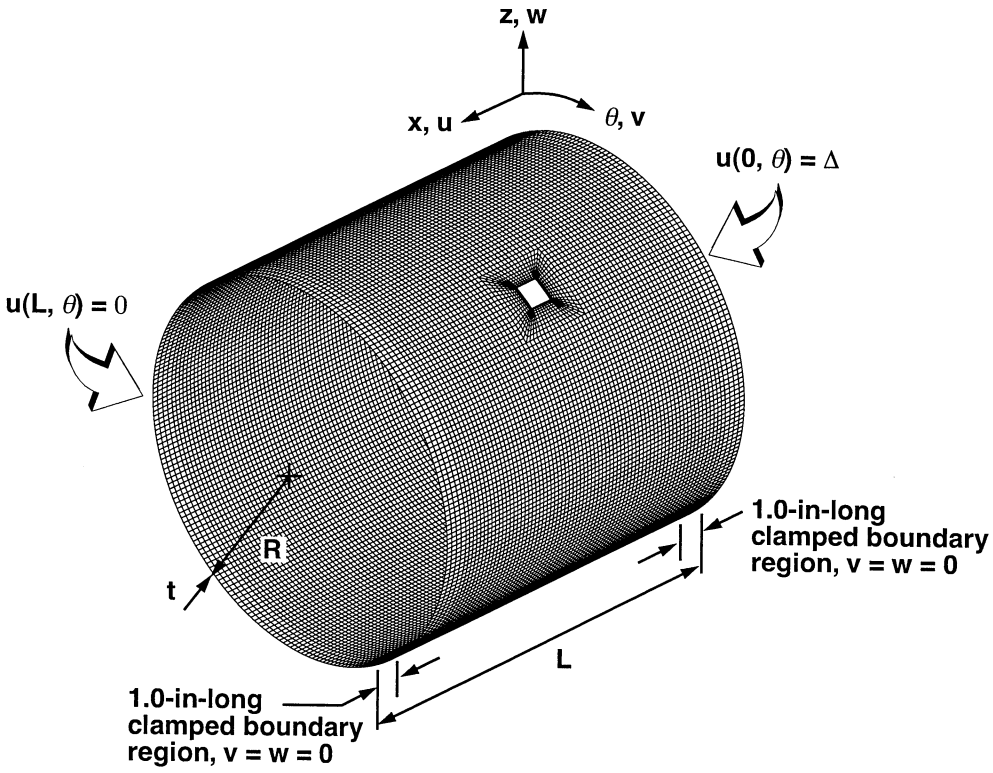

Fig. 1 Typical finite-element model geometry and boundary conditions.

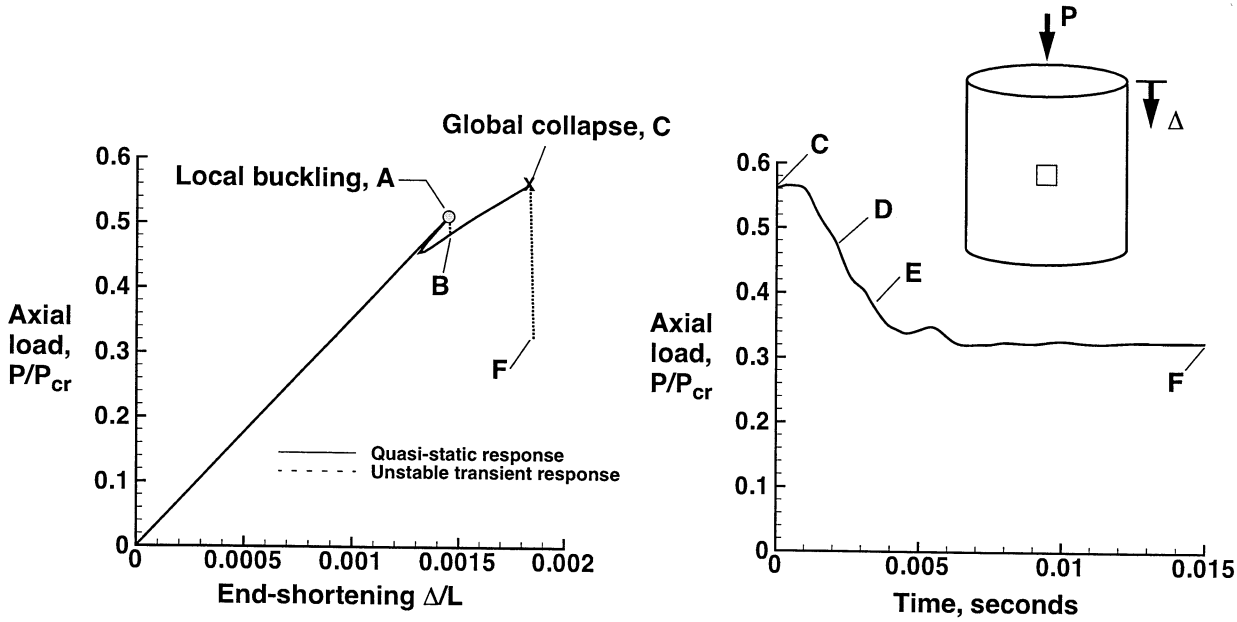

a) Load-shortening response

b) Load-time history during collapse

Fig. 2 Numerically predicted nonlinear response of a compression-loaded cylindrical shell with an unreinforced cutout C1.

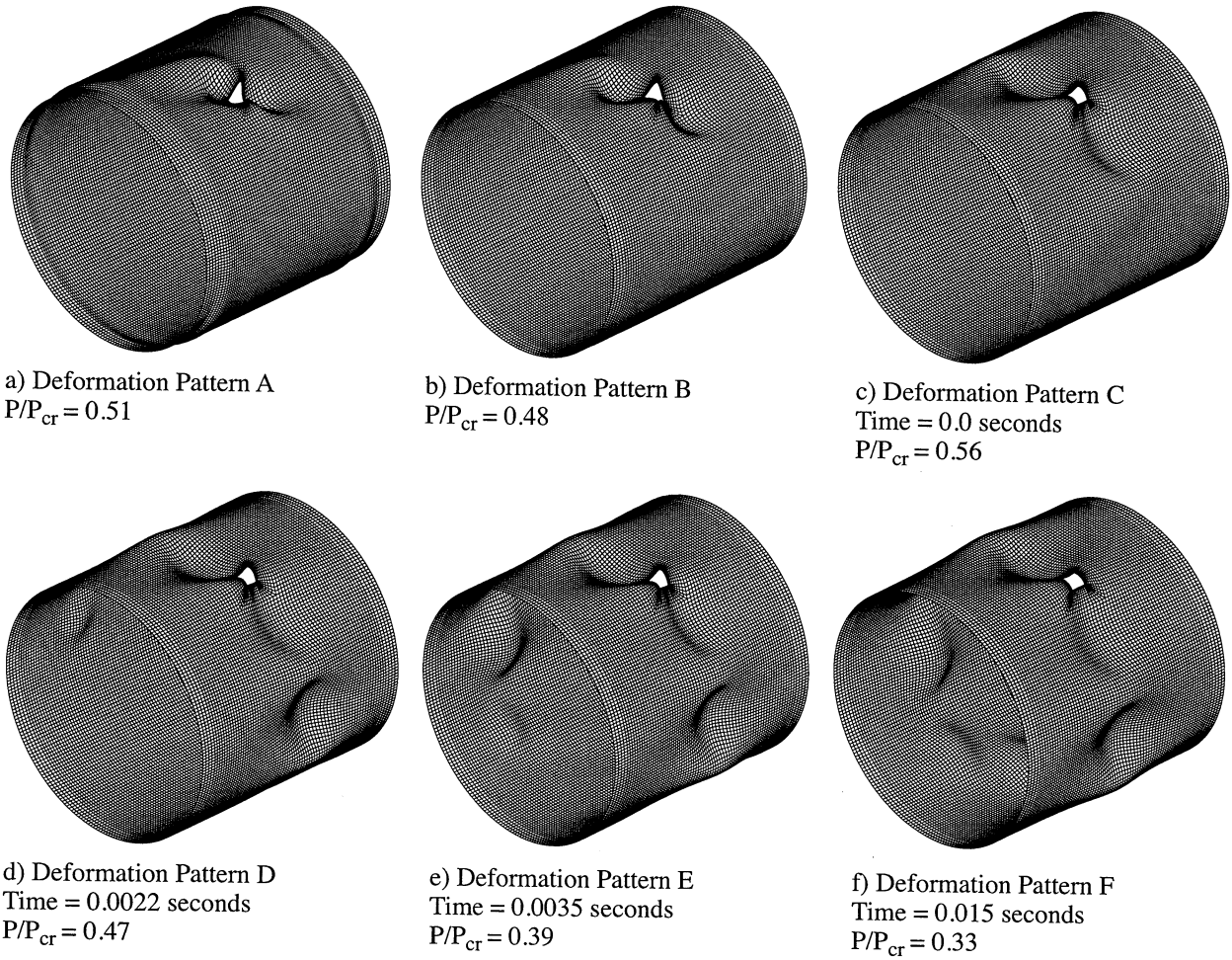

a) Deformation Pattern A
$P/P_{cr} = 0.51$

b) Deformation Pattern B
$P/P_{cr} = 0.48$

c) Deformation Pattern C
Time = 0.0 seconds
$P/P_{cr} = 0.56$

d) Deformation Pattern D
Time = 0.0022 seconds
$P/P_{cr} = 0.47$

e) Deformation Pattern E
Time = 0.0035 seconds
$P/P_{cr} = 0.39$

f) Deformation Pattern F
Time = 0.015 seconds
$P/P_{cr} = 0.33$

Fig. 3 Numerically predicted deformation response of a compression-loaded cylindrical shell with an unreinforced cutout C1. The deformation patterns A-F correspond to the points labeled in Fig. 2.

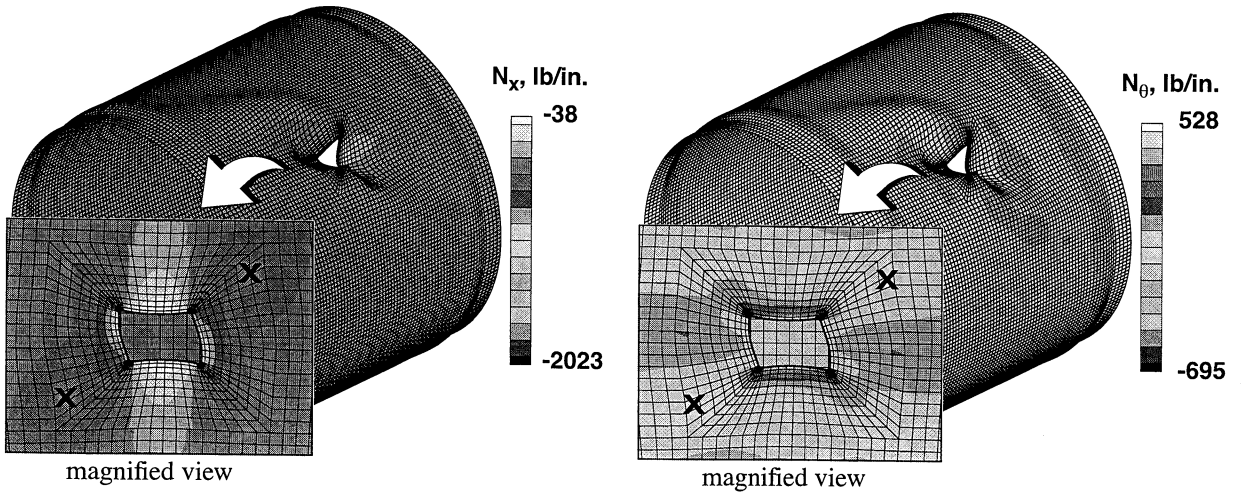

a) Initial local buckling, corresponding to Point A in Fig. 2a, $P/P_{cr} = 0.51$.

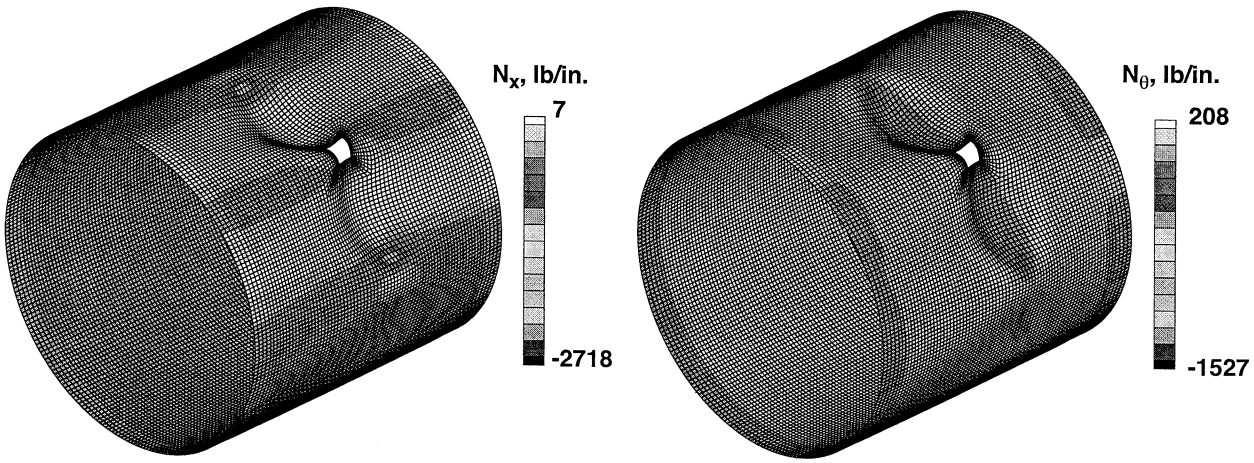

b) Initial global collapse, corresponding to Point C in Fig. 2a, $P/P_{cr} = 0.56$, time = 0.0 seconds.

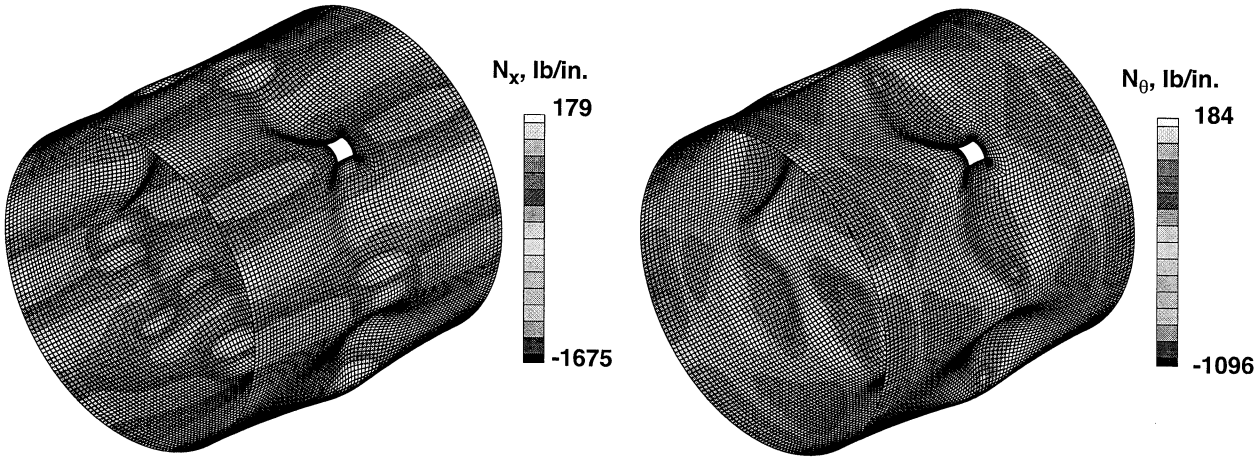

c) Post collapse, corresponding to Point F in Fig. 2a, $P/P_{cr} = 0.33$, time = 0.015 seconds.

Fig. 4 Numerically predicted deformation response and stress resultant contours at selected points in the non-linear response of a compression-loaded cylindrical shell with an unreinforced cutout C1.

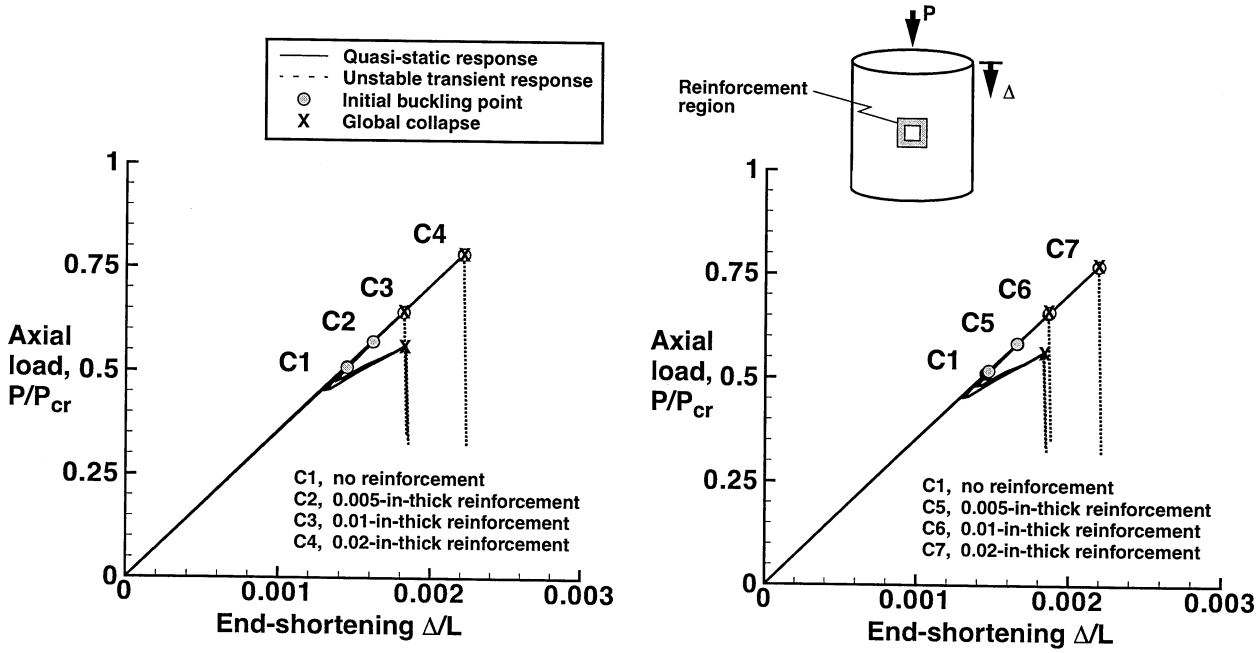

a) 0^o-ply orientation

b) 90^o-ply orientation

Fig. 5 Effects of cutout-reinforcement thickness and reinforcement fiber orientation on the predicted load-shortening response of a geometrically perfect compression-loaded cylindrical shell with a cutout. (2.4-in square-shaped reinforcement)

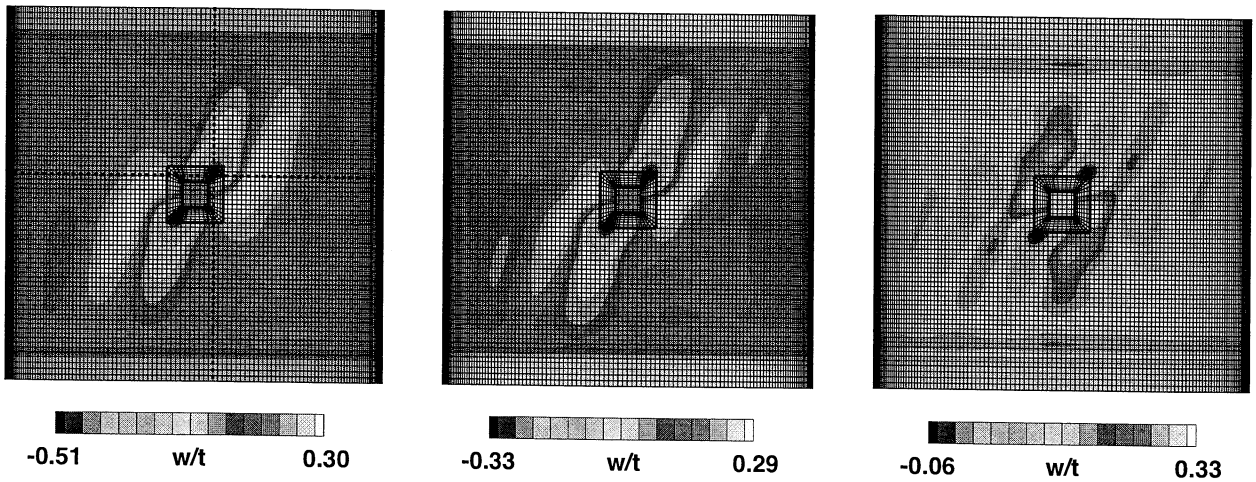

a) 0.005-in-thick reinforcement

b) 0.01-in-thick reinforcement

c) 0.02-in-thick reinforcement

Fig. 6 Effects of cutout-reinforcement thickness on the predicted initial-buckling deformations of a geometrically perfect compression-loaded cylindrical shell with a cutout. The reinforcement is a 2.4-in. square reinforcement with 0^o-ply orientation (the outer boundary of the reinforcement region is marked in the figures).

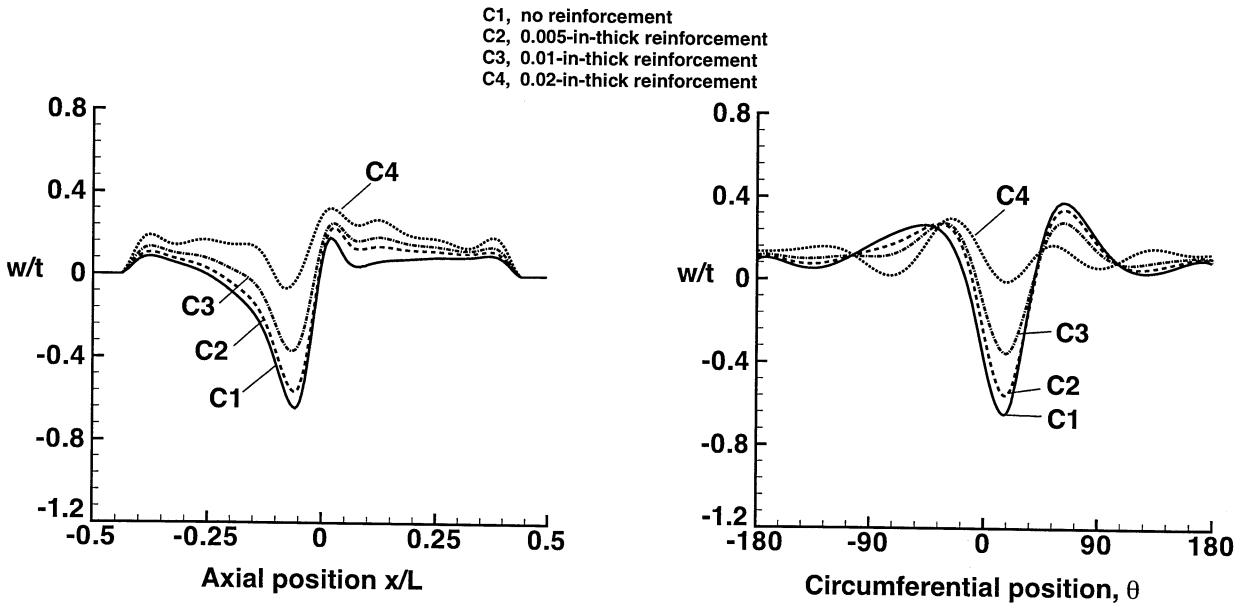

Fig. 7 Effects of cutout-reinforcement thickness on the radial-displacement response of a geometrically perfect compression-loaded cylindrical shell with a cutout. The reinforcement is a 2.4-in. square-shaped reinforcement with 0^{o}-ply orientation. The location of the axial and circumferential traces are indicated in Fig 6a

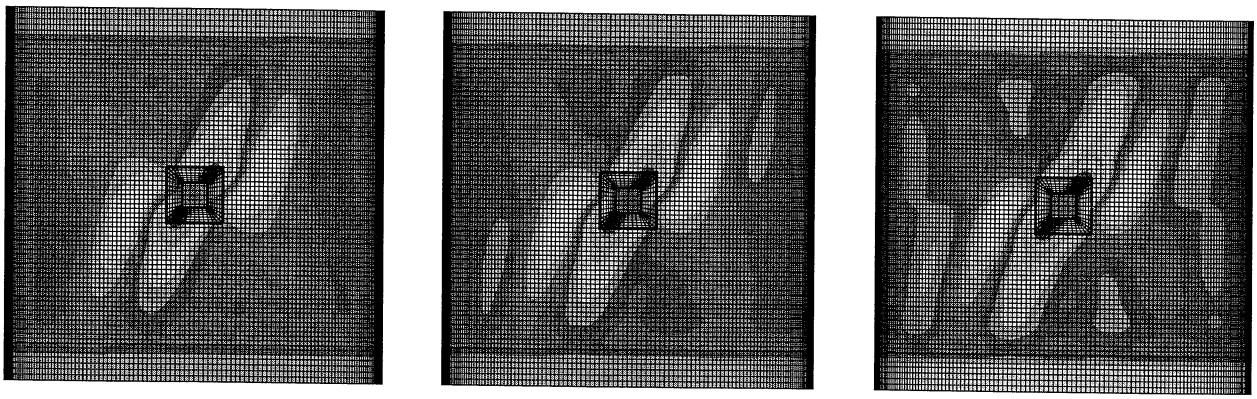

a) 0.005-in-thick reinforcement

b) 0.01-in-thick reinforcement

c) 0.02-in-thick reinforcement

Fig. 8 Effects of cutout-reinforcement thickness on the predicted initial-buckling deformations of a geometrically perfect compression-loaded cylindrical shell with a cutout. The reinforcement is a 2.4-in. square-shaped reinforcement with 90^{o}-ply orientation (The outer boundary of the reinforcement region is marked in the figures).

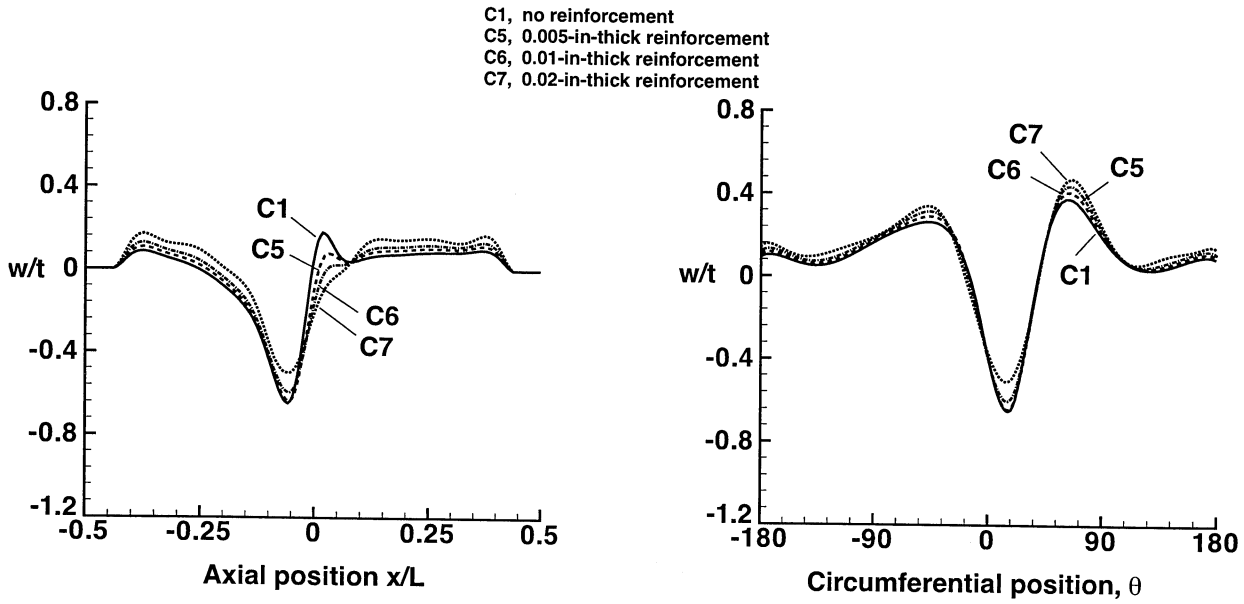

Fig. 9 Effects of cutout-reinforcement thickness on the radial-displacement response of a geometrically perfect compression-loaded cylindrical shell with a cutout. The reinforcement is a 2.4-in. square-shaped reinforcement with 90°-ply orientation. The location of the axial and circumferential traces are indicated in Fig 6a.

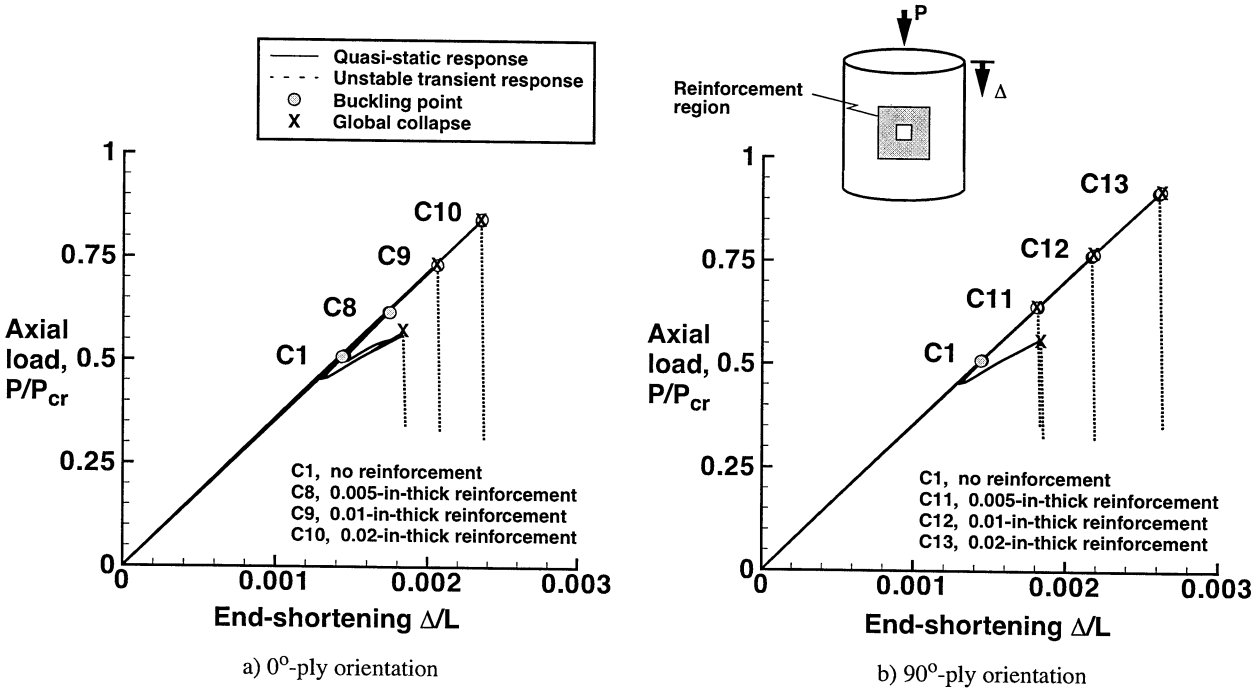

a) 0°-ply orientation

b) 90°-ply orientation

Fig. 10 Effects of cutout-reinforcement thickness and reinforcement fiber orientation on the predicted load-shortening response of a geometrically perfect compression-loaded cylindrical shell with a cutout. (4.4-in square-shaped reinforcement)

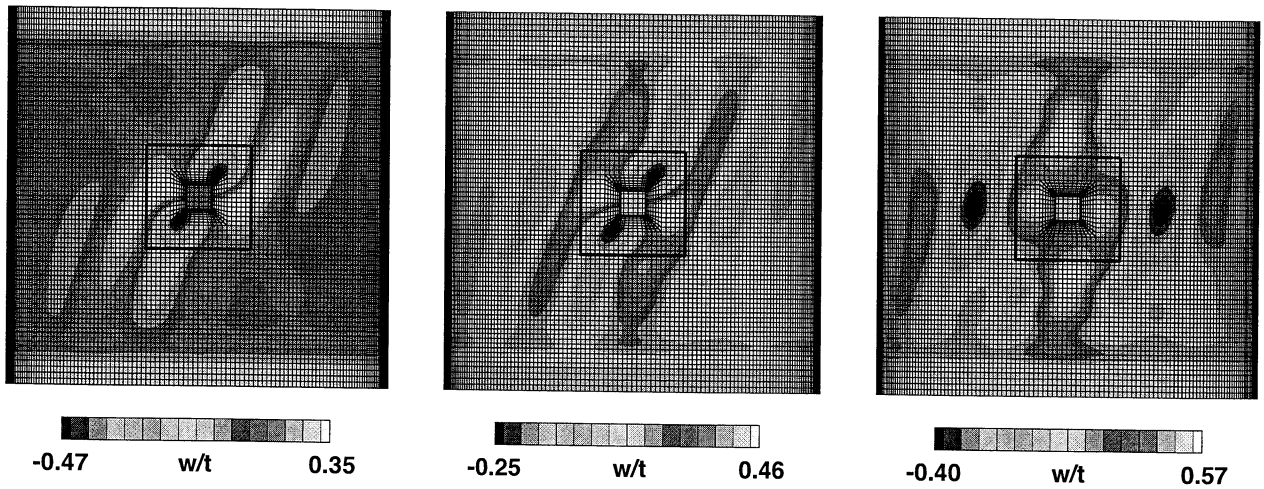

a) Shell C8, 0.005-in-thick reinforcement b) Shell C9, 0.01-in-thick reinforcement c) Shell C10, 0.02-in-thick reinforcement

Fig. 11 Effects of cutout-reinforcement thickness on the predicted initial-buckling deformations of a geometrically perfect compression-loaded cylindrical shell with a cutout. The reinforcement is a 4.4-in. square-shaped reinforcement with 0^o-ply orientation (the outer boundary of reinforcement region is marked in the figures).

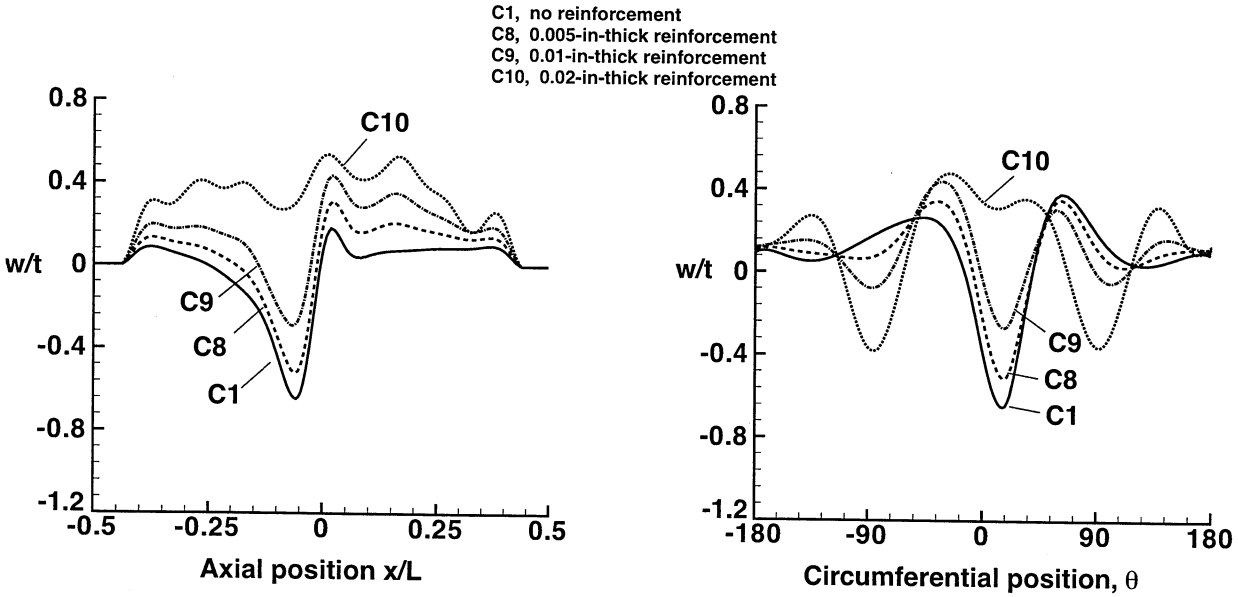

Fig. 12 Effects of cutout-reinforcement thickness on the radial-displacement response of a geometrically perfect compression-loaded cylindrical shell with a cutout. The reinforcement consists of a 4.4-in. square-shaped reinforcement with 0^o-ply orientation. The location of the axial and circumferential traces are indicated in Fig 6a.

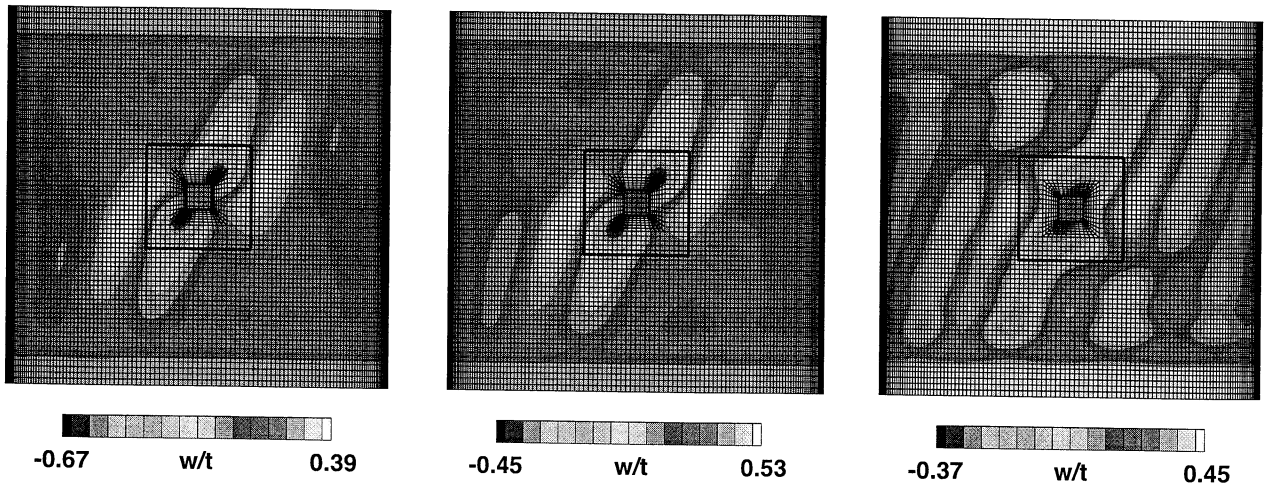

a) Shell C11, 0.005-in-thick reinforcement b) Shell C12, 0.01-in-thick reinforcement c) Shell C13, 0.02-in-thick reinforcement

Fig. 13 Effects of cutout-reinforcement thickness on the predicted initial-buckling deformations of a geometrically perfect compression-loaded cylindrical shell with a cutout. The reinforcement is a 4.4-in. square-shaped reinforcement with 90°-ply orientation (the outer boundary of reinforcement region is marked in the figures).

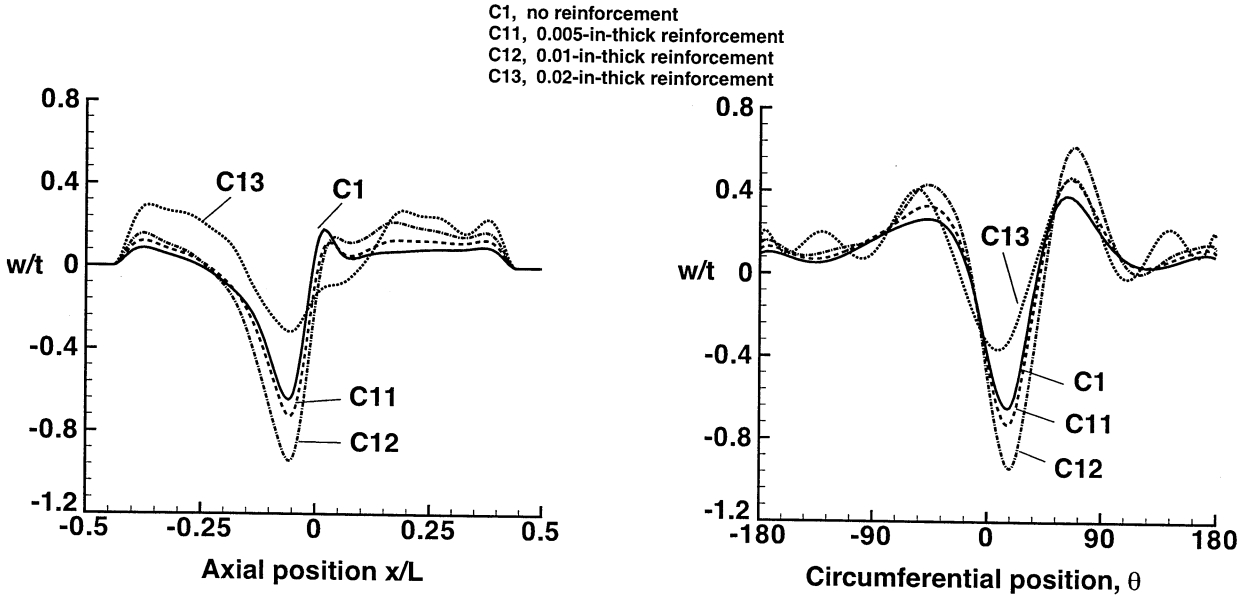

Fig. 14 Effects of cutout-reinforcement thickness on the characteristic radial-displacement response of a geometrically perfect compression-loaded cylindrical shell with a cutout. The reinforcement consists of a 4.4-in. square-shaped reinforcement with 90°-ply orientation. The location of the axial and circumferential traces are indicated in Fig 6a.

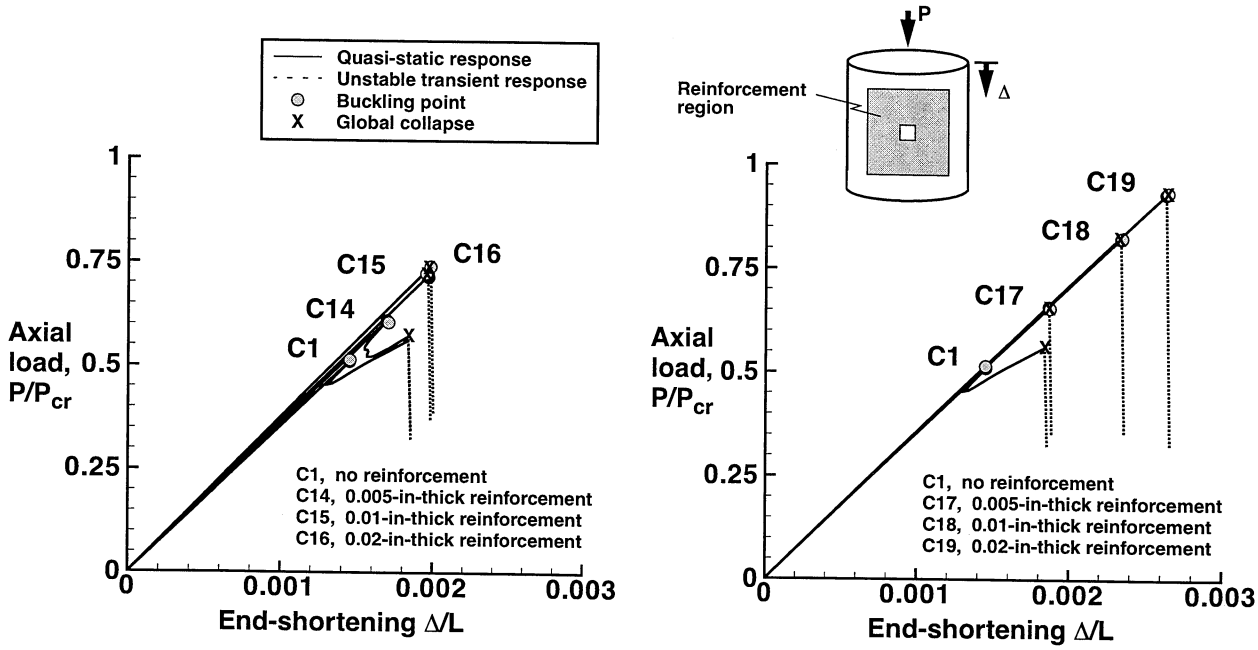

a) 0^{o}-ply orientation

b) 90^{o}-ply orientation

Fig. 15 Effects of cutout-reinforcement thickness and reinforcement fiber orientation on the predicted load-shortening response of a geometrically perfect compression-loaded cylindrical shell with a cutout. (8.0-in square-shaped reinforcement)

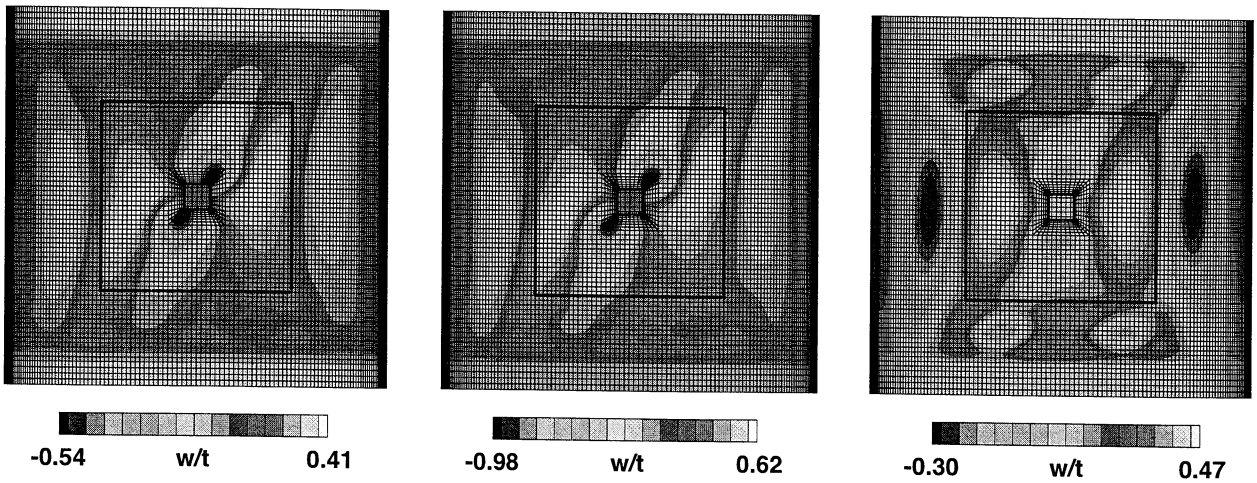

a) Shell C14, 0.005-in-thick reinforcement b) Shell C15, 0.01-in-thick reinforcement c) Shell C16, 0.02-in-thick reinforcement

Fig. 16 Effects of cutout-reinforcement thickness on the predicted initial-buckling deformations of a geometrically perfect compression-loaded cylindrical shell with a cutout. The reinforcement is a 8.0-in. square-shaped reinforcement with 0^{o}-ply orientation (the outer boundary of reinforcement region is marked in the figures).

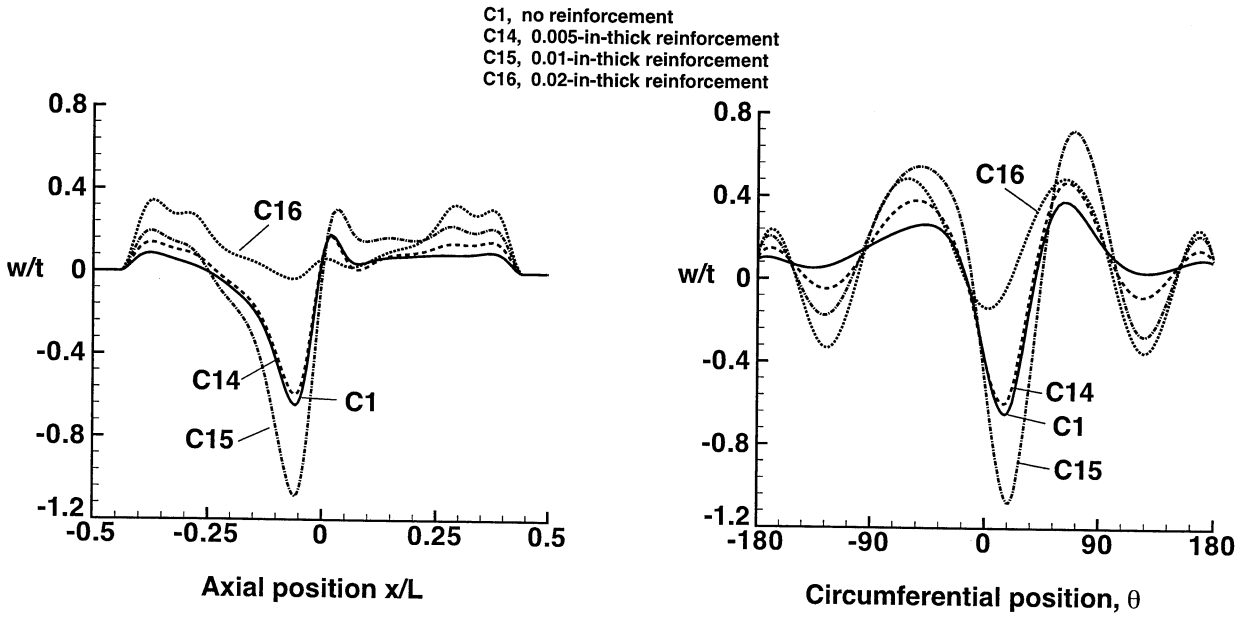

Fig. 17 Effects of cutout-reinforcement thickness on the radial-displacement response of a geometrically perfect compression-loaded cylindrical shell with a cutout, The reinforcement consists of a 8.0-in. square-shaped reinforcement with 0^0-ply orientation, The location of the axial and circumferential traces are indicated in Fig 6a.

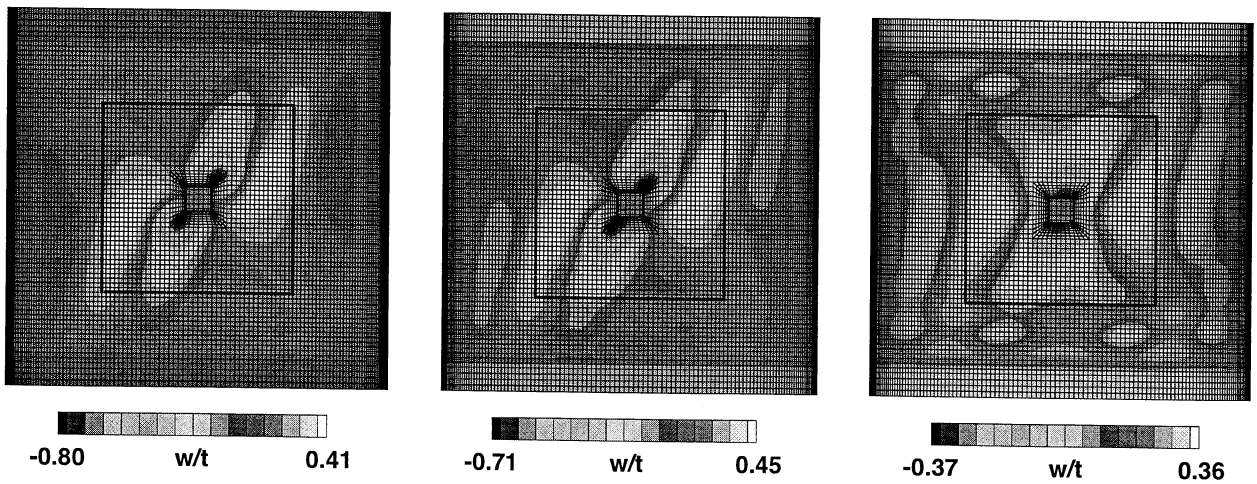

a) Shell C17, 0.005-in-thick reinforcement b) Shell C18, 0.01-in-thick reinforcement c) Shell C19, 0.02-in-thick reinforcement

Fig. 18 Effects of cutout-reinforcement thickness on the predicted initial-buckling deformations of a geometrically perfect compression-loaded cylindrical shell with a cutout. The reinforcement is a 8.0-in. square-shaped reinforcement with 90^0-ply orientation (the outer boundary of reinforcement region is marked in the figures).

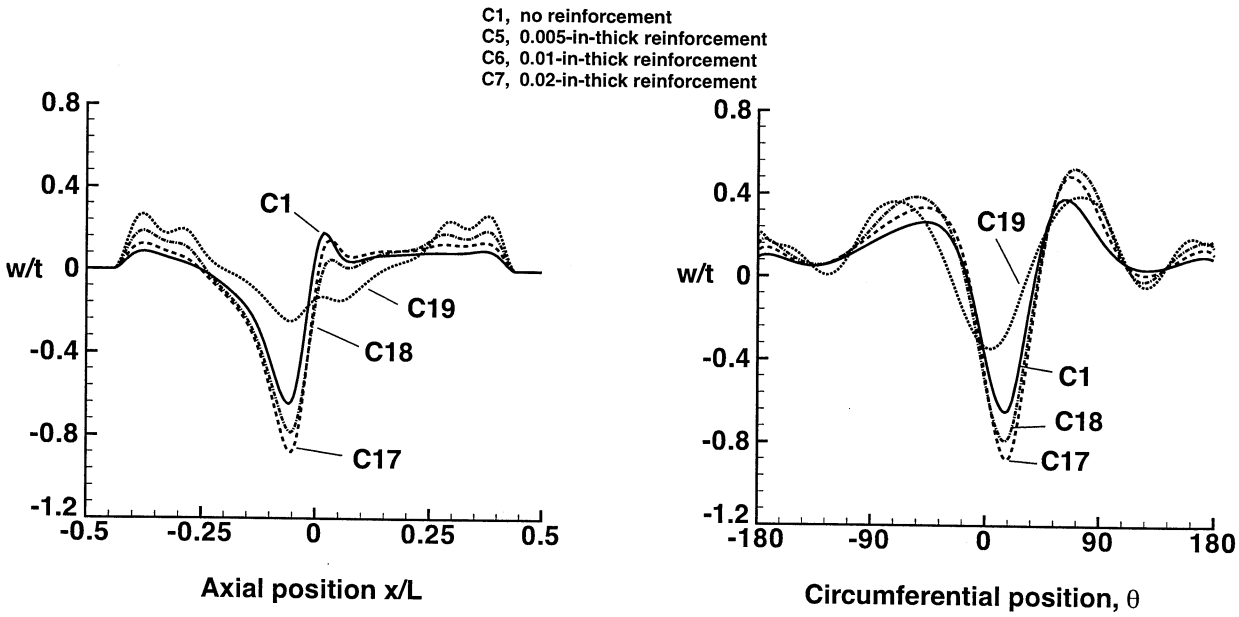

Fig. 19 Effects of cutout-reinforcement thickness on the radial-displacement response of a geometrically perfect compression-loaded cylindrical shell with a cutout. The reinforcement consists of a 8.0-in. square-shaped reinforcement with 90^{o}-ply orientation. The location of the axial and circumferential traces are indicated in Fig 6a.